Published in final edited form as:

Sci Signal. 2024 May 28; 17(838): eado6266. doi:10.1126/scisignal.ado6266.

Hippo and PI5P4K signaling intersect to control the transcriptional activation of YAP

Lavinia Palamiuc[1], **Jared L. Johnson**[2,5], **Zeinab Haratipour**[3,6], **Ryan M. Loughran**[1], **Woong Jae Choi**[3], **Gurpreet K. Arora**[1], **Vivian Tieu**[1], **Kyanh Ly**[1], **Alicia Llorente**[1], **Sophia Crabtree**[1], **Jenny C.Y. Wong**[2,7], **Archna Ravi**[1], **Thorsten Wiederhold**[4], **Rabi Murad**[1], **Raymond D. Blind**[3,*], **Brooke M. Emerling**[1,*]

[1]Sanford Burnham Prebys, La Jolla, CA 92037

[2]Weill Cornell Medicine, Meyer Cancer Center, New York, NY 10021

[3]Vanderbilt University Medical Center, Department of Medicine, Division of Diabetes, Endocrinology and Metabolism, Nashville, TN 37232

[4]Cell Signaling Technology, Inc., Danvers, MA 01923

[5]Weill Cornell Medicine, Department of Medicine, New York, NY 10021

[6]Austin Peay State University, Clarksville, TN, 37044

[7]New York University Grossman School of Medicine, Department of Cell Biology, New York, NY 10016, USA

Abstract

Phosphoinositides are essential signaling molecules. The PI5P4K family of phosphoinositide kinases and their substrates and products, PI5P and PI4,5P_2, respectively, are emerging as intracellular metabolic and stress sensors. We performed an unbiased screen to investigate the signals that these kinases relay and the specific upstream regulators controlling this signaling node. We found that the core Hippo pathway kinases MST1/2 phosphorylated PI5P4Ks and inhibited their signaling in vitro and in cells. We further showed that PI5P4K activity regulated several Hippo- and YAP-related phenotypes, specifically decreasing the interaction between the key Hippo proteins MOB1 and LATS and stimulating the YAP-mediated genetic program governing epithelial-to-mesenchymal transition. Mechanistically, we showed that PI5P interacted with MOB1 and enhanced its interaction with LATS, thereby providing a signaling connection between the Hippo pathway and PI5P4Ks. These findings reveal how these two important evolutionarily conserved signaling pathways are integrated to regulate metazoan development and human disease.

*Correspondence: ray.blind@vanderbilt.edu (R.D.B.); bemerling@sbpdiscovery.org (B.M.E.).

Author contributions: L.P, J.L.J., R.D.B. and B.M.E. conceived the project and designed experiments. L.P, J.L.J., Z.H., R.M.L., W.J.C., G.K.A., V.T., K.L., J.C.Y.W., A.R. and T.W. designed experiments and performed the research. L.P, J.L.J., Z.H., R.M.L., G.K.A., V.T., J.C.Y.W., A.R., T.W., R.M., R.D.B. and B.M.E. analyzed the data. L.P., J.L.J., R.D.B. and B.M.E. wrote the manuscript. All authors approved the final version of the manuscript.

INTRODUCTION

Phosphoinositides are a group of seven distinct species of phospholipids generated by the phosphorylation of the third, fourth and fifth positions of the inositol headgroup of phosphatidylinositol(1). The seven resulting phosphoinositides are cycled and regulated by a complex network of kinases and phosphatases that add or remove phosphate groups at specific positions. Phosphoinositide signaling impacts many cellular processes, including proliferation, survival, and growth, and its dysregulation is common in cancer and other diseases. One of the least studied phosphoinositide species is the low abundance phosphatidylinositol 5-monophosphate (PI5P), which, 20 years after its discovery, has yet to be definitively linked to any specific cellular pathway. PI5P is the lipid substrate for the type II phosphatidylinositol-5-phosphate 4-kinases (PI5P4Ks) and was the last phosphoinositide to be discovered (2). PI5P4Ks phosphorylate PI5P at the 4-position to generate distinct pools of phosphatidylinositol 4,5-bisphosphate ($PI4,5P_2$). The importance of this evolutionarily conserved pathway for generating $PI4,5P_2$, as well as for cycling PI5P, is still poorly understood. To date only a few PI5P4K regulators have been identified, including the kinases p38 MAPK(3) and mTOR(4). Similarly, the list of characterized binders to PI5P remains short. These binders are ING2(5), which connects nuclear PI5P to p53-dependent apoptosis; TOM1(6), which is involved in endosomal maturation; and Tiam1(7), which is related to cell migration and invasion.

Several phospholipids regulate the Hippo pathway (8–12), which consists of four major kinases, mammalian Ste20-like kinases 1 and 2 (MST1/2) and large tumor suppressor LATS1 and LAT2 (LATS1/2), as well as the associated adaptor proteins SAV and MOB1. The main downstream target of Hippo pathway, Yes-associated protein (YAP), activates various transcriptional programs related to cell growth. YAP dysregulation has been linked to various pathologies including cancer and cancer metastasis (13). Here, we provide a previously unrecognized connection between PI5P4K activity and Hippo pathway regulation. We identified MST1 and MST2 as direct inhibitors of PI5P4Ks. PI5P4K knockdown or knockout led to enhanced activity downstream of MST1/2 and decreased activity of YAP. Thus, our study reveals insights into how PI5P4Ks relay metabolic information to the Hippo pathway. PI5P4Ks are druggable kinases (14–22) and therefore, these data can be leveraged in targeting diseases with dysregulated Hippo signaling, such as cancers.

RESULTS

The MST kinases control intracellular turnover of $PI4,5P_2$ by directly phosphorylating PI5P4Ks

To identify new direct regulators for PI5P4Ks, we conducted in vitro kinase assays in which we incubated the lipid kinase PI5P4Kβ with a panel of protein kinases and ATP. Then, we included the lipid substrate PI5P with radio-labeled ATP and measured the generation of $PI4,5P_2$ by thin layer chromatography (TLC) (Fig. S1A). Of the approximately 29 kinases assayed, the Hippo pathway core kinase MST1 had the most potent effect on PI5P4Kβ, completely inhibiting its activity in a concentration-dependent manner (Fig. 1A, Fig. S1B). In addition, we found that MST1 also inhibited the activity of the PI5P4Kα isoform (Fig.

1A). MST1 is a germinal center kinase II (GCKII) protein, part of the “STE20-like” family of proteins that play essential roles as regulators of cell fate and cell growth. Other germinal center kinase family members also inhibited PI5P4Kβ, including MST2 (Fig. 1B), HGK, GLK, MST3 and TAOK1 (Fig. S1C). Moreover, we found this effect to be evolutionarily conserved because the human MST1 inhibited the activity of the *Caenorhabditis elegans* PPK-2 orthologue for PI5P4Ks (Fig. S1D). Finally, this regulation was specific to type II PI5P4Ks because MST1 did not affect the activities of type I PI4P5Ks (Fig. S1E). MST1/2 are serine-threonine protein kinases (23). The best characterized substrates for MST1/2 are MOB1A, MOB1B (24, 25), LATS1, and LATS2 (26), the core members of the classical Hippo cascade. Other substrates include NDR1/NDR2 (27), FOXO1 (28), and FOXO3a (29). Our initial observations indicated that MST1/2 kinase function inhibited the in vitro activity of PI5P4K. Indeed, we showed by SDS-PAGE autoradiography direct phospho-transfer by MST1 to both PI5P4Kα and PI5P4Kβ in vitro (Fig. 1C).

We next sought to validate that MST1/2 phosphorylated and inhibited PI5P4Ks in cells. To measure the activity of PI5P4K, we visualized $PI4,5P_2$ by immunofluorescence using a commercially available antibody as an indicator of PI5P4K activity. To distinguish from $PI4,5P_2$ generated by the activity of the largely plasma membrane-localized type I PI4P5Ks, we specifically examined intracellular $PI4,5P_2$, which is predominantly generated by the activity of type II PI5P4Ks. Using this approach we measured intracellular $PI4,5P_2$ in HEK 293A cells with CRISPR/Cas9-mediated knockout (KO) for both MST1 and MST2 (MST KO, Fig. S1F). In support of the in vitro data, we observed a significant increase in intracellular $PI4,5P_2$ in the cytoplasm of MST KO cells compared to WT cells (Fig. 1D). This effect was rescued by expression of functional WT MST1 (MST1 WT(30)), but not by that of a kinase dead mutant MST1 (MST KD (30)) (Fig. 1D). Further, we observed a similar pattern in *Mst1*$^{-/-}$*Mst2*$^{+/-}$ mouse embryonic fibroblasts (MEFs)(31) (Fig. S1G). We measured a 2.6-fold increased accumulation of intracellular $PI4,5P_2$ in *Mst1*$^{-/-}$*Mst2*$^{+/-}$ MEFs as compared to WT MEFs (Fig. S1H).

We next identified and validated the MST1 phosphorylation site on the PI5P4Ks. MST1 is threonine-specific and prefers aliphatic residues at the +1 position and basic residues, especially lysine, at the +2 position (T-[aliphatic]-K)(32). Thr^{376} in PI5P4Kα and Thr^{386} in PI5P4Kβ fit MST1’s motif criteria and are located in the substrate binding sites (Fig. S1D). This site and the surrounding sequence are mostly conserved in the *C. elegans* orthologue (Fig. S1D) and is not present in type I PI4P5Ks (Fig. S1E). To determine if this was the regulatory phosphorylation site, we repeated the in vitro kinase assay for PI5P4Kβ, comparing the activity of PI5P4Kβ WT with that of either a phospho-null T386A PI5P4Kβ or a phospho-mimetic T386D PI5P4Kβ mutant. First, the phospho-mimetic mutant showed no basal activity, consistent with the inhibitory effects of phosphorylation (Fig. 1E). Second, the phospho-null mutant was insensitive to MST1 treatment, consistent with Thr^{386} being the targeted site (Fig. 1E). Finally, to explore this regulatory mechanism in cells, we raised polyclonal antibodies against the MST1 threonine phosphorylation sites on the PI5P4Ks. To validate these antibodies (PI5P4K-P(K-T-K) #1, #2, #3, Fig. S1I), we expressed either human WT PI5P4Kα and PI5P4Kβ or the phospho-null T376A PI5P4Kα and T386A PI5P4Kβ in *Pip4k2a*$^{-/-}$*Pip4k2b*$^{-/-}$ (αβDKO) MEFs. We confirmed that the antibodies recognized PI5P4Kα and PI5P4Kβ WT but not their respective phospho-null

mutants (Fig. S1I). Using this tool, we assessed the phosphorylation of human PI5P4K α_FLAG and β_FLAG in WT and MST KO HEK 293A cells and measured a significant decrease in phosphorylation at this site in MST KO cells as compared to WT cells (Fig. 1F). This suggests that the phosphorylation of PI5P4Kα and PI5P4Kβ at Thr^{376} and Thr^{386}, respectively, depends on the activity of cellular MST1/2. Based on these data, we propose that MST1/2 potently inhibits PI5P4K activity by directly phosphorylating Thr^{376} in PI5P4Kα and Thr^{386} in PI5P4Kβ.

PI5P links PI5P4K signaling to the Hippo pathway

Because MST1/2 can inhibit PI5P4Ks, we asked if the resulting change in PI5P4K activity and PI5P/PI4,5P_2 ratio influenced the functional output of Hippo signaling downstream of MST1/2. We tested this hypothesis with MEFs isolated from WT or *Pip4k2a*$^{flx/flx}$*Pip4k2b*$^{-/-}$ (αβ DKO) mice. First, we measured the phosphorylation of the adaptor protein MOB1 and found a significant increase in MOB1 phosphorylation in αβ DKO cells compared to WT cells, indicating activated Hippo signaling (Fig. 2A). A similar effect was also observed in HEK293A cells with CRISPR/Cas9-generated KO for both PI5P4Kα and PI5P4Kβ (αβ DKO, Fig. S2A). High confluency activates MST1/2 and increase MOB1 phosphorylation. As expected, MOB1 phosphorylation was enhanced with increasing confluency in WT MEFs, whereas αβ DKO MEFs showed no further increase in MOB1 phosphorylation (Fig. S2B). Because MST1/2 inhibited PI5P4K activity, we further investigated if the observed increase in MOB1 phosphorylation depended on PI5P4K catalytic activity by re-expressing mouse WT PI5P4Kα (PI5P4Kα WT) or a kinase dead D359N PI5P4Kα (PI5P4Kα KD) mutant in αβ DKO MEFs. MOB1 phosphorylation was partially restored by re-expression of PI5P4Kα WT but remained unchanged by re-expression of PI5P4Kα KD (Fig. 2A). We next performed streptavidin bead pull-downs for MOB1 tagged with a streptavidin binding protein tag (SBP) transiently transfected into WT and αβ DKO HEK 293A cells. MOB1-LATS binding significantly increased upon PI5P4K loss, suggesting an increase in MOB1-LATS activity (Fig. 2B).

Because PI5P4Ks control intracellular pools of PI5P, we hypothesized that the increased MOB-LATS binding in the absence of the most active isoforms of PI5P4Ks may be mediated by PI5P, the substrate of these kinases. Phospholipids regulate components of the Hippo pathway (8–12), although LATS does not appear to bind to PI5P or PI4,5P_2 (9). Therefore, we focused our attention on MOB1. We first used a commercially available PIP array blotted with decreasing amounts of phosphoinositides and observed that Myc-tagged MOB1 immunoprecipitated with PI5P to the greatest degree among all mono-phosphoinositides tested and only showed weak interaction to diphosphoinositide (PI4,5P_2) and triphosphoinositide (PI3,4,5P_3) (Fig. 2C).

Positively charged surfaces within protein structures are important for phospholipid-protein interactions (33). We identified basic residues clustered within the N-terminus of MOB1 that could be responsible for binding to PI5P (Fig. 2D). To determine if altering these residues influences MOB1 interaction with PI5P, we purified recombinant forms of both full-length MOB1 and a N-terminal truncated MOB1 lacking the first 32 amino-acids (MOB1 ΔN-term), which also harbors Thr^{12}, one of the MST1/2 phosphorylation residue.

We used these proteins to blot commercially available PIP strips spotted with various phospholipids, including PI5P and $PI4,5P_2$. Consistent with the PIP array results, full-length MOB1 interacted with the monophosphoinositides PI3P and PI5P to the greatest extent and less so with $PI4,5P_2$ (Fig. 2D). In contrast, the truncated version of MOB1 did not bind to monophosphoinositides (Fig. 2D). We mutated the positive residues within this region (Arg^8, Lys^{11}, Lys^{14}, Lys^{16}, and Lys^{17}) to alanine and examined two mutated residues at a time (K11/14A and K16/17A) as well as all the 5 positively charged residues together (5A mutant, MOB1 5A). Two mutations simultaneously (K11/14A and K16/17A) reduced the PI5P binding on PIP strips but mutating all 5 positively charged residues had a more pronounced effect with the MOB1 5A mutant showing little detectable binding to PI5P (Fig. S2C). Together, these studies are consistent with MOB1 binding to solid-phase PI5P and suggest the binding depends on the presence of basic residues in the N-terminus.

Attempts to co-crystalize the MOB1-PI5P complex failed; thus, computational docking and molecular dynamics (MD) simulations were used to examine these interactions with an AlphaFold2-based model of full-length MOB1 (Fig. S2D). Blind, rigid-body computational docking to MOB1 predicts that PI5P binds to MOB1 with lower energy than $PI4,5P_2$ (Fig. 2E), with the acyl chains located in a hydrophobic pocket of MOB1 (Fig. S2D). Interaction of PI5P with MOB1 remained stable throughout a 50ns MD simulation (Movie S1). In contrast, $PI4,5P_2$ interaction with MOB1 became unstable after just 23ns into the simulation, with the acyl chains adopting a rigid conformation and the headgroup moving away from the MOB1 protein (Movie S2). PI5P induced less root mean square deviation (RMSD) in MOB1 structure than did $PI4,5P_2$ over the course of the simulation (Fig. 2F). Fluctuation of individual MOB1 residues was similar in the PI5P and $PI4,5P_2$ simulations (Fig. 2G, S2E), except at the N-terminus of MOB1 where PI5P induced less fluctuation (Fig. 2G. S2E). The PI5P ligand itself also fluctuated to a lesser extent than the $PI4,5P_2$ ligand over the simulation, with largest differences in atoms of the inositol headgroup (atoms 62–91) and the sn2 acyl chains (atoms 92–139, Fig. 2H). All computationally docked structures of PI5P to MOB1 predicted the acyl chains to be buried in a hydrophobic cleft of MOB1, with residues of the N-terminus protecting the acyl chains from solvent (Fig. 2I). Docked models of the MOB1-PI5P interaction predict that Arg^8 of MOB1 interacts with the 5-position phosphate of PI5P headgroup, whereas Lys^{11}, Lys^{14}, and Lys^{16} do not (Fig. 2I). PyRx docking to multiple crystal structures of the MOB1-LATS complex (PDB:5B5W and PDB:5BRK) predicts that PI5P binds to MOB1-LATS with lower computed energy than does $PI4,5P_2$, regardless of which crystal structure was used for docking (Fig. S2F-G). Moreover, according to these docked models, PI5P is predicted to bind at the interface between MOB1 and LATS, establishing contact with both proteins. This alignment is consistent with the stabilization of the MOB1-LATS interaction in PI5P4K null cells by exogenous PI5P (Fig. 2B). Together, these data suggest that PI5P interacts with MOB1 in a manner dependent on positively charged residues in the N-terminus of MOB1, an activity we did not observe for $PI4,5P_2$ in silico. Thus, our data suggest MOB1 selectively interacts with the PI5P4K reaction substrate over the PI5P4K reaction product, consistent with PI5P acting as a second messenger that connects PI5P4K signaling to the Hippo pathway.

Downregulation of YAP activation upon PI5P4K inhibition

The activation of the MOB1-LATS complex leads to phosphorylation of YAP(34), which prevents YAP from translocating to the nucleus and promotes its proteasomal degradation(35–37). Therefore, we next tested whether PI5P4K silencing resulted in increased YAP phosphorylation and decreased nuclear translocation. Inhibition of proteasomal degradation with MG132 significantly increased YAP phosphorylation in αβ DKO MEFs compared to WT MEFs (Fig. 3A). Further, re-expressing PI5P4Kα WT in αβ DKO MEFs decreased YAP phosphorylation, whereas YAP phosphorylation was restored to WT levels in αβ DKO MEFs expressing PI5P4Kα KD, supporting that the kinase activity of PI5P4Ks are necessary for YAP activation (Fig. 3A). YAP is the effector of the Hippo pathway and when dephosphorylated, YAP translocates to the nucleus where it activates various target genes through its interaction with transcription factors such as TEADs(38, 39). The YAP transcriptional program is essential for development(37) and has been linked to various human diseases such as cancer. To measure the activation of the TEAD transcription factor(40), we expressed the TEAD promotor region fused with luciferase ($TEAD^{luc}$), which revealed that TEAD activation was decreased in αβ DKO as compared to WT HEK 293A cells (Fig. 3B). Moreover, increasing cell density conditions in WT cells correlated with decreasing luciferase intensity, suggesting a decrease in TEAD activity. However, that decrease was less marked in αβ DKO HEK293A cells (Fig. 3B). To confirm these observations, we analyzed YAP localization. By immunofluorescence analysis, we measured an approximately 30% decrease in the nuclear/cytoplasmic YAP ratio in αβ DKO as compared to WT MEFs (Fig. S3A). As observed above with MOB1 phosphorylation, higher confluency decreased YAP nuclear localization in WT cells but did so to a lesser extent in αβ DKO cells (Fig. S3B). Similarly, we generated MCF10A human breast epithelial lines in which we deleted PI5P4Kα by CRISPR/Cas9 gene editing and PI5P4Kβ by a doxycycline (DOX)-inducible shRNA ($\alpha^{-/-}$;β sh_in, Fig. S3C). Consistent with our results in MEFs, $\alpha^{-/-}$;β sh_in MCF10A cells also showed a decrease in the nuclear:cytoplasmic YAP ratio, which was partially rescued upon re-expression of human PI5P4Kα WT, but not by that of PI5P4Kα KD (Fig. 3C). This observation further validates that the kinase activity of PI5P4Ks has an important role in modulating the Hippo pathway. We next asked whether silencing PI5P4Ks was sufficient to inhibit YAP activity in human cancer cell lines. We stably suppressed PIP4K2B with shRNA and silenced PI5P4K2A with two different PIP4K2A hairpins (α sh_1/β sh, α sh_2/β sh) in both HCC1806 breast cancer cells and in SKOV3 ovarian cancer cells (Fig. S3D). As suggested by our observations in MEFs and in MCF10A cells, YAP nuclear protein amounts were reduced and the nuclear:cytoplasmic ratios were lower in the α sh_1/β sh, α sh_2/β sh lines in both cancer lines when compared to controls (Fig 3D and Fig. S3E).

To confirm the inhibition of YAP activity by PI5P4Ks, we measured the gene expression of two classical YAP target genes *Ccn2* (which encodes CTGF) and *Ccn1* (which encodes CYR61) (38), which were significantly decreased in αβ DKO MEFs (Fig. S3F). To further understand the downstream effects of silencing PI5P4Ks on YAP activity, we performed RNA sequencing (RNA-seq) analysis to compare gene expression. Gene set enrichment analysis (GSEA) of the genome-wide dataset revealed a significant decrease in the expression of the Cordenonsi YAP signature gene list (41) in $\alpha^{-/-}$;β sh_in MCF10A

cells (Fig. 3E) and in α sh_1/β sh, α sh_2/β sh relative to control cells (Fig. 3F). In MCF10A cells, some of the top hits were genes encoding for growth factors such as *TGFB2* and *FGF2* and were confirmed by qPCR (Fig. 3G). To validate the importance of PI5P4Ks in regulating YAP transcriptional activity, we overexpressed either PI5P4Kα or PI5P4Kβ (Fig. S3G) in MCF10A cells, both of which increased the expression of these genes (Fig. S3H). Moreover, in HCC1806 cells, one of the top hits identified was the gene encoding the tyrosine kinase receptor *AXL*, a metastasis driver in human cancers (42, 43), and the gene encoding *SLIT2*, a modulator of cancer cell migration (44, 45). We confirmed this strong decrease in gene expression of the genes encoding *CCN2*, *SLIT2* and *AXL* by qPCR analysis (Fig. 3H). In ovarian cancer cells, we also measured reduced expression of the genes encoding *CCN2, CCN1* and *SLIT2* (Fig. S3I). Together, these observations demonstrate the regulation of YAP transcriptional activity by PI5P4Ks in cancer cells.

PI5P4Ks regulate the functional output of the Hippo pathway

Because several hits identified in the RNA-seq datasets have been implicated in various aspects of epithelial to mesenchymal transition (EMT)(46), a YAP-driven program, we performed GSEA analyses for the standard EMT signature (Hallmark Epithelial to Mesenchymal Transition). Indeed, in both MCF10A and the HCC1806 breast cancer cell line, the EMT signature was enriched in control groups compared to groups lacking or with reduced PI5P4K expression (Fig. S4A). In MCF10A DKO cells, the expression of the gene encoding the EMT driver TWIST1 was decreased in our RNA-seq data set, which was confirmed by qPCR analysis (Fig. 3G). YAP activates *TWIST1* transcription, along with other EMT drivers (47). The top hits for decreased expression in HCC1806 cells with decreased PI5P4K expression included genes encoding vimentin, FN1, and CDH2 (N-cadherin), known markers of EMT (Fig. S4A). A standard indicator of EMT is loss of the cell adhesion protein E-cadherin. YAP and E-cadherin are tightly linked: YAP has been proposed to be a target of E-cadherin and conversely, YAP can alter the activity of E-cadherin through its transcriptional targets as well as through protein-protein interaction with the small GTPase RAC1. $\alpha^{-/-}$;β sh_in MCF10A cells showed a 1.5-fold increase in E-cadherin immunofluorescence, an increase that was partially reversed by expression of WT PI5P4Kα, but not kinase-dead PI5P4Kα, again emphasizing the importance of kinase activity (Fig. 4A). Next, we assessed EMT phenotypes that are transcriptionally regulated by YAP(46, 48), specifically migration and invasion. Migration was examined by wound healing assays, which showed that $\alpha^{-/-}$;β sh_in cells had a significantly decreased migration speed compared to SCR cells after wounding (Fig. 4B). We also examined migration capacity in HCC1806 breast cancer cells. Cells with double knock-down of PIP4K2A and PIP4K2B migrated approximately 50% less than control cells (Fig. 4C). Next, we analyzed the in vitro invasiveness of MCF10A cells stimulated with a serum gradient, which revealed that a significantly lower percentage of $\alpha^{-/-}$;β sh_in cells invaded through the matrigel membrane when compared to SCR MCF10A cells (Fig. 4D). A similar difference was observed in α^{sh_1}/β^{sh} and α^{sh_2}/β^{sh} HCC1806 cells when compared to controls **(Fig. 5E)**. These data support the decrease in the expression of EMT-related genes as shown by RNA-seq analyses and collectively demonstrate that PI5P4K ablation inhibits the YAP pathway as well as YAP-related phenotypes.

To assess the potential relevance of this PI5P4K-Hippo pathway interaction to human cancers, we correlated the two signatures (Cordenonsi YAP conserved signature and hallmark EMT) and *PIP4K2A* expression in human patients with invasive breast carcinoma from the TCGA Pan-Cancer Atlas data base. Higher expression of *PIP4K2A* correlated with significantly higher expression of YAP and EMT signatures (Fig. S4B). Using the same data set, we further confirmed that *CCN2*, *CCN1*, *AXL* and *SLIT2* expression positively correlated with *PIP4K2A* expression (Fig. S4C). Finally, we extended our correlative analysis between *PIP4K2A* expression and the Cordenonsi YAP conserved signature (Fig. S4D) and the hallmark EMT signature (Fig. S4E) to other human cancers and again observed significant and strong positive associations in ovarian, colorectal adenocarcinoma, prostate and head and neck cancers. These correlative analyses hint at the utility of future studies regarding the potential role of PI5P4Ks in YAP-driven cancers.

DISCUSSION

The present work highlighted the core Hippo pathway kinases MST1/2 as direct regulators of PI5P4Ks and revealed a role for PI5P4Ks in regulating the Hippo pathway. Inhibition of the PI5P4Ks stimulated MOB1 phosphorylation and formation of the MOB1-LATS complex. This correlated with increased YAP phosphorylation and decreased nuclear localization. Finally, we found that YAP-related phenotypes were reduced by PI5P4K deficiency, thus demonstrating that these phosphoinositide kinases play a role in regulating YAP function.

Finding upstream regulators for PI5P4Ks will enhance our understanding of the cellular roles PI5P4Ks and phosphoinositide regulation. PI5P4Ks are regulated by only a small number of protein kinases, with cellular stress being a common denominator. The stress MAP4K p38 is the only known kinase that directly phosphorylates Thr^{326} in PI5P4Kβ, which inhibits its activity in response to UV irradiation stress, leading to an increase in nuclear PI5P(3). Similarly, the isomerase Pin1 decreases PI5P4K activity(49). Our efforts led to the identification of the core Hippo pathway kinases MST1/2 and other GCKs as specific inhibitors of the activity of PI5P4Ks. Both enzymatically active isoforms PI5P4Kα and PI5P4Kβ seem to ultimately be inhibited by cellular stressors, which leads to increased PI5P(49, 50). This body of previous work makes the case for PI5P as a secondary messenger for stress signaling. Another regulator of PI5P4Ks highlighted here is HPK/GCK-like kinase (HGK/MAP4K4), which directly interacts with and activates LATS1(51). In fact, MST1/2 is dispensable for LATS1/2 activation and can be replaced by other regulators such as HGK/MAP4K4, suggesting a degree of redundancy in the regulation of the Hippo pathway. Thus, at least two kinases that impinge on the Hippo pathway can also regulate PI5P4Ks. Further research will be necessary to determine the degree to which HGK/MAP4k4 utilizes PI5P to enhance LATS1/2 activation and inhibit YAP activity.

MST1/2 are protein kinases central to cellular stress responses(29, 52–54). They can be regulated by cell-cell contact, oxidative stress(29), energy(54) and growth factors(55, 56). Thus, we propose that, by activating MST1/2, stress can stimulate an increase in PI5P pools by attenuating PI5P4K activity. To support this hypothesis, we showed that knocking down PI5P4Ks also promoted MOB1-LATS complex formation. Activation of MST1/2 leads to

inhibition of YAP nuclear translocation and activity. Indeed, knocking down PI5P4Ks led to reduction of YAP nuclear translocation and YAP gene expression signatures, which could not be rescued by a kinase dead PI5P4K. Together, our data support a role for PI5P4K activity in regulating the functional output of the classical Hippo pathway by PI5P signaling. Lastly, we demonstrate that PI5P4Ks affected YAP-related phenotypes, more specifically in regulating the EMT program. Indeed, YAP regulates EMT(57, 58) and various EMT drivers(47), along with phenotypes such as migration and invasion(48). YAP overexpression induces EMT(58), whereas YAP inhibition can stop EMT progression(57). In the same way, ablation of PI5P4Ks in MCF10A epithelial cells and breast cancer cells reduced EMT gene signatures and invasion and migration.

PI5P is the least abundant phosphoinositide in the cell. There are several lipid kinases and phosphatases that directly contribute to PI5P synthesis. Three 3-phosphatases (MTM1, MTMR2 and MTMR3) likely produce PI5P from $PI3,5P_2$. PIKfyve is a 5-kinase that contributes to PI5P biosynthesis by phosphorylating PI3P to $PI3,5P_2$. Finally, 4-phosphatases I and II recycle PI5P from $PI4,5P_2$. Some of these enzymes stimulate EMT events such as invasion and migration. For instance, PIKfyve regulates the invasion of cells through TIAM-1-dependent cytoskeletal regulation(7). However, TIAM1 also antagonizes YAP signaling and inhibits invasion of epithelial cells(59). Further, both PIKfyve and MTMR3 may promote invasion by activating Rac1(60) presumably through PI5P production. On the other hand, PI5P4Ks are 4-lipid kinases that consume PI5P and have been suggested to affect cellular processes by turning over PI5P rather than through their product, $PI4,5P_2$, due to the lower abundance of PI5P compared to that of $PI4,5P_2$. Our data propose one such mechanism for PI5P4Ks in regulating PI5P pools available for the Hippo pathway activation which, to a certain extent, does not fully agree with more established roles for PI5P. These observations highlight the complexity of phospholipid regulation. Although phospholipid dynamics is still not fully understood, the functions of various phospholipids are predicted to be context-dependent in terms of subcellular localization or physiological condition. It remains unclear how MOB1 might acquire phospholipid ligand. As an initial hypothesis, MOB1 might be expected to interact with membrane lipids not unlike how phosphatidylinositol-transfer proteins (PITP)(61–64) or phosphoinositide-binding nuclear receptors (SF-1)(65–68) acquire phospholipids. Although the details of how PITPs acquire phospholipids is better defined(63), how proteins like SF-1 or MOB1 might accomplish this task are almost completely uninvestigated.

Furthermore, whether lipids are localized at the plasma membrane, internal membranes and potentially lipid rafts, and the other lipid kinases and phosphatases in the vicinity will most likely dictate phospholipid dynamics and function. Cellular localization could prove essential to the cellular roles for PI5P. Likewise, studying the different lipid kinases involved in regulating PI5P and their dynamics and interactions in specific cellular contexts could further our understanding of PI5P biology. Overall, our study uncovered putative PI5P4Ks regulators as well as a previously unknown signaling cascade. Although PI5P4Ks are relevant in various disease contexts such as cancer, the mechanisms and pathways are still not fully understood. Our study highlights a connection between PI5P4Ks and the Hippo pathway, with potential implications for development and cancer biology.

MATERIALS AND METHODS

Cell lines

All cells were incubated in a 37°C humidified incubator with 5% CO_2. Mouse embryonic fibroblasts (MEFs) and human epithelial kidney (HEK) 293A cells were cultured in Dulbecco's modified Eagle medium (Corning 10–013-CV). Media was supplemented with 10% fetal bovine serum (Life Technologies), 100 U/ml penicillin/streptomycin (Gibco; 15140122). MCF10A human breast epithelial cells were grown in DMEM/F-12 medium (Gibco; 11330032) supplemented with 5% horse serum (Gibco 16050122), 20ng/ml EGF (Sigma-Aldrich; E9644), 10μg/ml insulin (Sigma-Aldrich; I1882), 100ng/ml cholera toxin (Sigma-Aldrich; C8052), 0.5mg/ml hydrocortisone (Sigma-Aldrich; H0888) and 100 U/ml penicillin/streptomycin.

MEFs were isolated from E13.5 embryos and genotyped as described previously(69). *Pip4k2a*$^{flx/flx}$*Pip4k2b*$^{-/-}$ MEFs were infected at a MOI=10 of FIVCMVCre VSVG to knockout *Pip4k2a* from the lines and generate *Pip4k2a*$^{-/-}$*Pip4k2b*$^{-/-}$ MEFs (αβ DKO MEFs). Rescue lines expressing mouse WT PI5P4Kα (α WT) and kinase-dead PI5P4Kα D359N (α KD) were also generated by retroviral infection. For MCF10A cells, *PIP4K2A* was initially deleted using CRISPR and cells were lentivirally infected with a doxycycline-inducible shRNA targeting *PIP4K2B* and selected in 2ug/ml puromycin. To generate MCF10A lines lacking both isoforms of the kinases, cells were treated with 3ug/ml doxycycline for 3 consecutive days before carrying out experiments in the presence of doxycycline. The *PIP4K2A*$^{-/-}$*;PIP4K2B*$^{-/-}$ HEK 293A cell line was generated using CRISPR as previously described (70). MCF10A breast epithelial mCherry CT, mCherryPI5P4Kα (α OE) and mCherryPI5P4Kβ (β OE) fusion overexpression lines were generated by lentiviral infection of MCF10A cells with pRRL mCherry, pRRL mCherry-PIP4K2A and pRRL mCherry-PIP4K2B. Infected cells were selected using mCherry fluorescence by fluorescence activated cell sorting (FACS).

The cancer cell lines HCC1806, SKOV3 and HCC116 were purchased from ATCC. PIP4K2B was stably knocked down by lentiviral transduction of shRNA. HEK293T cells were cotransfected with 12 μg of each shRNA containing pLKO.1 plasmid, 8 μg of psPAX2 packaging plasmid, and 4 μg of pMD2.G envelope plasmid using Lipofectamine 2000 (Invitrogen) in 10-cm plates. After 16 h, medium was replaced with fresh 10% FBS-DMEM without antibiotics, and 48 h later, the viral supernatant was collected and filtered through a 0.45-μm filter. HCC1806, SKOV3 and HCC116 cells were transduced with viral supernatant and 8 μg/ml polybrene, and stably infected cells were selected with 1 μg/ml puromycin. Knockdown of PIP4K2A was performed prior to each experiment. One day after seeding, cells were transduced with either control or αsh1 or αsh2 shRNA (Day 0). After 24 hours puromycin was added to the growth at a concentration of 1 ug/ml (Day 1). After 48 hours of selection cells were seeded for the respective experiments on day 3 after infection.

The 293T packaging cell line was used for retroviral and lentiviral amplification. In brief, viruses were collected 48 hours after transfection, filtered, and used for infecting cells in the presence of 10μg/ml polybrene (Santa Cruz Biotechnology; NC9840454) prior to puromycin selection or upon cell sorting for mCherry. pCL-Ampho and pCL-Eco were used

for retroviral packaging for human and mouse cells respectively. pVSVg and pPax were used for lentiviral packaging. MST1/ MST2 CRISPR double knock-out (MST KO) HEK293A cells were a kind gift from Dr. Kun Lian Guan(51).

Coimmunoprecipitation

Cells were transfected with either MOB1B or LATS1 with a C-terminal SFB tag (S-tag;Flag-tag; Streptavidin Binding Protein-tag). Plasmids were transfected using Lipofectamine™2000 reagent (Thermo Fisher Scientific 11668019) as per manufacturers recommendations. In brief, cells at 70–80% confluency were incubated for 4 hours at 37°C with Lipofectamine-DNA complex (2:1). Fresh media was added and cell were incubated for 24 hours prior to treatment and processing. Cells were lysed in IP buffer (25mM Tris 7.4, 150mM salt, 5% glycerol and 1% NP40) with Halt protease and phosphatase inhibitor cocktail (Thermo Fisher Scientific, 78440). Equal amounts of protein of each sample were incubated with pre-washed streptavidin magnetic beads (New England BioLab® S1420S) overnight at 4°C. Beads were thoroughly washed and the proteins were eluted under denaturing conditions in SDS-containing buffer and immunoblotted. MOB1B and LATS1 with a C-terminal SFB tag (S-tag;Flag-tag; Streptavidin Binding Protein-tag) or SFB alone kindly provided by Dr. Wenqi Wang.

In vitro kinase assay

For phosphorylation reactions, predetermined concentrations of protein kinase and lipid kinases were added to master mix containing 50 μM of ATP (Sigma), 0.1 mg/mL of BSA and 1x Assay Buffer I (SignalChem) in 40 μl total volumes. Reactions were carried out at 30°C for 30 minutes. Next, 0.01 mCi/mL ^{32}P-labeled ATP (Perkin Elmer) and 25 μM PI5P:PS or PI4P:PS liposomes (Avanti) were included in the kinase reaction, bringing total volume to 100 μL. Additional cold ATP was included to maintain its concentration at 50 μM. Lipid phosphorylation reactions were carried out at room temperature for 20 min. 50 μl of 4N HCl was added to quench the reaction and the lipid was extracted with 100 μl of CHCl3: MeOH (1:1) followed by vortexing for 1 minute and centrifugation at 14,000XG for 2 minutes. 10 μL of the lower hydrophobic phase was extracted with gel loading pipet tips and spotted onto a silica plate (EMD Millipore #M116487001) for thin layer chromatography. Plates were placed in a sealed chamber with 1-propanol: 2M acetic acid (65:35) mobile phase. After completion, the plates were removed, briefly dried, exposed to a storage phosphor screen BAS-IP (GE Life Sciences) and imaged with a Typhoon FLA 7000 phosphorimager (GE) and quantified by ImageQuant (GE). PI5P:PS or PI4P:PS liposomes were prepared by mixing lipid substrate with 2-fold mass excess PS in chloroform. The chloroform was evaporating with N_2 gas, and the lipid mixture was hydrated in 30 mM HEPES pH 7.4, 1 mM EGTA and dispersed by bath sonication.

In vitro phosphorylation

Predetermined concentrations of MST1 and PIP4K2A and PIP4K2B were incubated in 50 μM of ATP, 0.01 mCi/mL ^{32}P-labeled ATP (Perkin Elmer), and 1x Assay Buffer I (SignalChem) at 30°C for 30 minutes. Reactions were run on SDS-PAGE and stained with Coomassie. Bands corresponding to PIP4K2A and PIP4K2B were examined for radioactivity incorporation by imaging with a Typhoon FLA 7000 phosphorimager (GE).

MOB1 expression and purification

Full length wild type MOB1B (MOB1 WT, residues 1–223) and alanine mutant MOB1B (MOB1 5A, residues 1–223) were subcloned into a pET21a vector with a C-terminal 6XHIS tag with ampicillin selection. For MOB1 5A, mutated residues were all contained in the N-term (R8A, K16A, K19A, K21A, K22A). All constructs were transformed into BL21 DE3 bacteria and purified by affinity chromatography. Briefly, single clones were grown in LB media under ampicillin selection at 37°C until OD600 reached ~0.5. Cultures were chilled on ice, induced at OD600 = 0.6 with 1mM IPTG for 18hr at 14°C, shaking at 100RPM. Cells were harvested by centrifugation for 15min at 3,000xg and resuspended in lysis buffer (50mM Tris HCl (pH 8.0), 150mM NaCl, cOmplete Protease tablets, and 1mg/mL lysozyme). Lysates were incubated on ice for 1hr with gentle rocking prior to sonication at 70% power with Branson Sonicator equipped with a titanium microtip on ice at 4°C for 10 minutes. Lysates were centrifuged at 14,000xg for 60 minutes. Supernatants were incubated for 1hr with HisPur Ni-NTA metal affinity resin (Thermo Scientific). The beads were washed 2X with 10 column volumes (CV) of Buffer A (50mM Tris HCl (pH 8.0), 150mM NaCl, and 25mM imidazole) and loaded onto a gravity column, washed with 10CV of Buffer A and eluted with 2CV Buffer B (50mM Tris HCl (pH 8.0), 150mM NaCl, and 300mM imidazole). The eluate was dialyzed in QBuffer A (50mM Tris HCl (pH 8.0)) overnight at 4C and loaded onto a HiTrap Capto Q column (Cytiva) pre-equilibrated with 50mM Tris HCl (pH 8.0) and eluted with QBuffer A + 1M NaCl. Eluted fractions corresponding to MOB1 WT or MOB1 5A mutant were pooled and concentrated using a 4mL Amicon® 10kDa filter prior to being aliquoted and stored at −80C. All samples analyzed were from aliquoted, frozen samples, and native gel electrophoresis showed no change in native gel migration after 1 freeze thaw cycle. MOB1B sample protein sequence was confirmed to be full-length MOB1B by native mass spectrometry.

Structural modeling of disordered regions in full-length MOB1

The crystal structure of MOB1B (PDB:5B5V) has disordered regions at both the N- and C-termini and at residues 100–105. To repair these regions missing from the crystal structures for computational docking studies to the full-length MOB1B, the MOB1B crystal structure (PDB:5B5V) was modeled by several independent approaches, including DMPfold(71), RaptorX(72, 73), InteractiveROSETTA(74) and AlphaFold2(75). The structure derived from AlphaFold2(75) had the lowest overall energy and was most similar to 5B5V and other structures of MOB1B in the protein database (Alphafold2 model RMSD with PDB:4JIZ = 0.306Å; PDB:5B5W = 0.701Å; PDB:5BRK = 0.448Å; PDB:5YF4 = 1.208Å). The full length AlphaFold2 model was therefore used for computational docking studies.

Computational phosphoinositide docking

Prior to docking, all phosphoinositide ligands were prepared by completing 200 steps of an energy minimization protocol using a universal force field (UFF). Global, undirected docking of dipalmitoyl PI5P (C16:0/C16:0) (1-(1,2-dioctanoylphosphatidyl)inositol-5-phosphate) or dipalmitoyl PI4,5P_2 (C16:0/16:0) (1-(1,2-dihexadecanoylphosphatidyl)inositol-4,5-bisphosphate) to the AlphaFold2 predicted structure of full-length MOB1B was performed using python-based PyRx(76) in a box

defined as 55.9Å X 54.9Å X 57.0Å centered on the midpoint of the MOB1 protein (x = 0.68277982839, y = −3.4843207781, z = 0.510424592091). This global docking approach minimized investigator-driven bias toward any specific binding region within MOB1. For phosphoinositide docking to the MOB1/LATS complex, similar unbiased global docking of UFF-minimized PI5P (C16:0/C16:0) and PI4,5P_2 (C16:0/C16:0) to crystal structures of the MOB1-LATS complex (PDB:5B5W and PDB:5BRK) were performed, as above. For 5B5W, the box was defined as 43.8Å X 68.0Å X 69.2Å centered on the midpoint of the 5B5W crystal structure (x = 11.1273943743, y = 28.4483213519, z = 45.9137039229). For 5BRK, the box was defined as 50.3Å X 66.3Å X 64.6Å centered on the midpoint of the 5BRK crystal structure (x = 24.7530485596, y = 40.3357547512, z = 7.6352332862). All solvent-exposed regions of the MOB1 protein were accessible to ligand during all docking runs.

Molecular dynamics simulations

To compare dynamics of PI5P and PI4,5P_2 binding to MOB1 WT and computationally test the stability of these interactions, we performed 50ns molecular dynamics (MD) simulations on MOB1 WT-PI5P and MOB1 WT-PI4,5P_2 complexes created by docking described above. Complexes were prepped for MD simulation using the CHARMM-GUI(77). Briefly, the complex was solvated in an octahedral box of explicit TIP3P water with a 10-Å buffer around the protein complex. A total of 26 potassium (K^+) and 22 Cl^- ions were added to neutralize the system charge and simulate physiologic conditions. SHAKE(78) bond length constraints were applied to all bonds involving hydrogen. Non-bonded interactions were evaluated with a 9-Å cutoff and calculated with a particle-mesh Ewald summation method(79, 80). The MD system was first minimized for 100 steps using steepest descent followed by 5,000 steps of conjugate gradient minimization. The system was heated to 300K over 125ps in the NVT ensemble using a step size of 1fs. After switching to the NPT ensemble, positional restraints on protein and ligand were gradually removed and Langevin dynamics with a collision frequency of 1.0ps^{-1} were used for temperature regulation. Production MD was conducted for 50ns using a step size of 2fs with constant pressure periodic boundary conditions, isotropic pressure scaling and Langevin dynamics. MD trajectories printed every 10ps and 5000 frames were created for further analysis. All minimizations and MD simulations were performed with Amber17(81) employing the ff14SB force field for proteins, GAFF2 force field for the phosphoinositide ligands, and the TIP3P force field for water molecules(82). Analysis of MD trajectories was performed using the CPPTRAJ module(83) of AmberTools. Root mean square deviations (RMSD) and root mean square fluctuations (RMSF) were calculated on all non-hydrogen atoms of protein residues for each frame in the trajectory using the initial structure as the reference. RMSF was also calculated for all atoms of PI5P and PI4,5P_2 for each frame in the trajectory, also using the initial state as the reference.

Immunofluorescence

PI4,5P_2 staining for intracellular membranes was done using the protocol described(84). In brief, cells were fixed in 2% pre-warmed methanol free PFA followed by permeabilization with 20 μM digitonin. Samples were blocked in 5% normal goat serum in buffer A (20mM PIPES pH 6.8, 2.7mM KCl, 137 mM NaCl) with 50mM NH_4Cl before being incubated

for 1hour at room temperature in primary antibody against $PI4,5P_2$ (1:100) (Echelon Biosciences; Z-P045–2). Samples were washed twice before incubation with secondary antibody for 45 min at room temperature, followed by post-fixation with 2% PFA in PBS. During the final washes, DAPI was added to the wash buffer. The samples were imaged with 40x oil objectives on a Zeiss LSM710 microscope. Total cell area and % area represented by $PI4,5P_2$ was quantified in ImageJ. For YAP (Cell Signaling Technology®, S14074 YAP (D8H1X) XP® rabbit monoclonal antibody) and E-cadherin (Proteintech, 60335–1 E-Cadherin rabbit monoclonal antibody) imaging, cells were fixed with 4% PFA and blocked in 0.3% Triton-X with 5% normal goat serum in PBS for 1hour at room temperature. Antibodies were diluted 1:100 in antibody dilution buffer (0.3% Triton-X with 1% BSA in PBS) and incubated overnight at 4C. Secondary antibodies were diluted 1:1000 in antibody dilution buffer and incubated for 1hour at room temperature. During the final washes, DAPI was added to the wash buffer. The samples were imaged with a 20X objective using the Biotech Imager. Average intensity was measured in Image J.

Western blotting

Cells were lysed with RIPA lysis buffer containing 1% Triton X-100, 0.1% SDS, 150 mM NaCl, 50 mM Tris-HCl pH 7.5 supplemented with Halt protease and phosphatase inhibitor cocktail (Thermo Fisher Scientific, 78440). Protein concentrations were quantified using the BCA method (Thermo Scientific; 23225) and 20μg of total cell lysates were run on an SDS–polyacrylamide gel electrophoresis. Proteins were transferred on to a nitrocellulose membrane, and membranes were probed overnight at 4°C with the appropriate primary antibody. See Table S1 for a complete list of antibodies used. Membranes were incubated with appropriate secondary antibodies and visualized using a LI-COR Odyssey® Imager. All quantifications were done using ImageJ.

PIP Array

PIP Array (P6100, Echelon) were incubated with recombinant human MOB1B C-MYC/DDK (TP306337, OriGene) and processed per the manufacturer's instruction. In brief, strips were blocked in 3% free fatty acid (FFA) BSA for 1H at room temperature and incubated with 0.5ug/ml of protein in 3% FFA BSA overnight at 4ºC. Strips were thoroughly rinsed in TBST and incubated for 2 hours at room temperature with Myc antibody, then with HRP-conjugated secondary antibody for 45 min. Standard Western blot developing procedures were followed.

PIP strips

PIP strips were incubated with recombinant MOB1B (XM-005265709) protein with a C-terminal 6X His tag (MOB1 WT construct made in Emerling lab; the three mutant MOB1 constructs, MOB1 K11/14A, MOB1 K16/17A and MOB1 5A, were synthesized by GENEWIZ). Proteins were expressed in competent *E. coli* BL21(D3) (New England BioLab® C2527). *E. coli* single colonies housing the appropriate plasmids were grown in LB cultures until O.D. = 600nm. Protein synthesis was induced with 0.5 mM IPTG at 18°C overnight. Protein extraction was done with B-PER™ Bacterial Protein Extraction Reagent (Thermo Scientific™ 78243) containing lysozyme (100ug/ml) and DNase I (5U/ml). Protein was isolated using Ni-NITA magnetic beads (New England Biolabs). Synthesized

proteins were visualized by SDS-PAGE and proteins were quantified using Quick Start™ Bradford Reagent (Bio-Rad 5000205). PIP strips (P6002, Echelon) were processed per the manufacturer's instructions. In brief, strips were blocked in 3% FFA BSA for 1H at room temperature. Following blocking, they were incubated with 10μg total protein 3% FFA BSA overnight at 4ºC. Strips were thoroughly rinsed in TBST and incubated for 2 hours at room temperature with His (Proteintech) antibody, then with secondary antibody (Li-COR) for 45 min. Standard Western blot developing procedures were followed.

RNA extraction and qPCR

Total RNA was prepared using Directzol RNA MiniPrep (Zymo Research Corporation; 50–444-628). cDNA was synthesized using High-capacity cDNA Reverse Transcription kit (ThermoFisher Scientific; 4368814) and qRT-PCR performed utilizing PowerUp SYBR green (ThermoFisher Scientific; A25742) and the LightCycler 96 (Roche). See Table S2 for a complete list of primers.

RNA sequencing and alignment

RNA was extracted from cell pellets washed with PBS using Directzol RNA MiniPrep (Zymo Research Corporation; 50–444-628). RNA yield and purity was tested using the Qubit 4 Fluorometer prior to analysis. Sequencing libraries were prepared using 250ng RNA using standard Illumina Tru-seq single indexing protocols and sequenced using the Illumina NextSeq 500 instrument. Adapter remnants of sequencing reads were removed using cutadapt v1.18(85). Read alignment was performed using human genome v.38 and Ensembl gene annotation v.84 using STAR aligner v.2.7(86). DESeq2 was used for differential gene expression analysis(87).

Gene set enrichment

Gene set enrichment analysis (GSEA) was performed using GSEA v4.0.3. Normalized enrichment scores (NES) and p values were used to determine the significance of findings.

Wound healing assay

Scratch assays were performed in 24 well plates. In brief, $3.5X10^5$ cells were plated in each well, three-four technical replicates per condition. 24 hours post-plating, the scratch was performed using an AutoScratch Wound Making Tool (BioTek). Cells were thoroughly washed and fresh media was added. Wound closure was monitored for 24 hours on a Cytation5 imager (BioTek) using the Scratch Assay App (BioTek). Wound area was measured using ImageJ.

Invasion assays

Invasion assays were performed in BioCoat™ Matrigel® Invasion Chambers (Corning; 354480) following the manufacturer's instructions. MCF10A cells were FBS-deprived overnight. Prior to plating, invasion inserts were rehydrated with FBS free media for 2 hours in a humidified tissue culture incubator at 37°C and 5% CO_2. Cells were resuspended in FBS free media at $1X10^5$ cell/ml. Chemoattractant media (media containing FBS) was added to the companion 24 well plates, and rehydrated inserts placed in the plate. Cells

were added to the inserts and incubated overnight. Cells were fixed with 70% ethanol for 20 minutes at room temperature, thoroughly washed with diH_2O and stained in a solution of 0.05% crystal violet for 30 minutes at room temperature. After thoroughly washing the excess stain, cells in the upper chamber were carefully removed with a cotton swab and the membranes were allowed to dry for at least 24 hours prior to mounting on microscopy slides. For each group, at least 2–3 technical replicates were assessed per experiment. Images were acquired using an Olympus microscope.

Statistics

Data are expressed as means SD. Data was verified for normality using Shapiro-Wilk normality test. Statistical analyses for all data, including microscopy quantification and qPCR were performed by Student's two-tailed t-test or ANOVA with Bonferroni's method used to correct for multiple comparisons, as indicated, using GraphPad Prism. Statistical significance is indicated in the figures. *$p<0.05$, **$p<0.001$, and ***$p<0.0001$ unless specified otherwise.

Supplementary Material

Refer to Web version on PubMed Central for supplementary material.

Acknowledgments:

We would like to thank the following cores at SBPMDI (NCI P30 CA030199): Cell Imaging and Histology, Flow cytometry, Bioinformatics and Genomics. At Vanderbilt we thank Markus Voehler and the NMR instrumentation core supported by NSF (0922862), NIH (S10 RR025677) and the computing cluster of the Advanced Center for Research and Education (ACCRE). We further thank Dr. Kun-Liang Guan for providing us with MST1/2 CRISPR KO HEK293A cell lines. We would also like to thank Dr. Wenqi Wang for sharing with us $MOB1^{SFB}$ and $LATS^{SFB}$ constructs.

Funding:

This work was supported by NCI (R01 CA237536), NIGMS (R01 GM143583), ACS (RSG-20-064-01-TBE), ACS (TLC–21–156–01) to B.M.E., and NCI (T32 CA211036) to R.M.L. Work in the R.D.B. laboratory was supported by ACS (RSG–17–063–01), ACS (TLC–21–156–01), V Foundation for Cancer Research Grant (V2016–015), NIGMS (R01 GM132592) and NCI (R21 CA243036) to R.D.B., NIDDK (T32 DK007673) to A.N.W., and NHGRI (T32 HG008341) to Z.H.

Competing interests:

J.L.J has received consulting fees from Scorpion Therapeutics and Volastra Therapeutics. The other authors declare that they have no competing interests.

Data and material availability:

The RNA-seq data have been deposited into the Gene Expression Omnibus (https://www.ncbi.nlm.nih.gov/geo/) with the accession ID GSE 221217. All other data needed to evaluate the conclusions in the paper are present in the paper or the Supplementary Materials. All materials are available from B. M. E. or R. D. B. upon reasonable request under a materials transfer agreement from Sanford Burnham Prebys and Vanderbilt University.

REFERENCES AND NOTES

1. Balla T, Phosphoinositides: tiny lipids with giant impact on cell regulation. Physiol Rev 93, 1019–1137 (2013). [PubMed: 23899561]
2. Rameh LE, Tolias KF, Duckworth BC, Cantley LC, A new pathway for synthesis of phosphatidylinositol-4,5-bisphosphate. Nature 390, 192–196 (1997). [PubMed: 9367159]
3. Jones DR, Bultsma Y, Keune W-J, Halstead JR, Elouarrat D, Mohammed S, Heck AJ, D'Santos CS, Divecha N, Nuclear PtdIns5P as a transducer of stress signaling: an in vivo role for PIP4Kbeta. Mol Cell 23, 685–695 (2006). [PubMed: 16949365]
4. Mackey AM, Sarkes DA, Bettencourt I, Asara JM, Rameh LE, PIP4kγ is a substrate for mTORC1 that maintains basal mTORC1 signaling during starvation. Sci Signal 7 (2014), doi:10.1126/SCISIGNAL.2005191/SUPPL_FILE/7_RA104_SM.PDF.
5. Bua DJ, Martin GM, Binda O, Gozani O, Nuclear phosphatidylinositol-5-phosphate regulates ING2 stability at discrete chromatin targets in response to DNA damage. Scientific Reports 2013 3:1 3, 1–9 (2013).
6. Boal F, Mansour R, Gayral M, Saland E, Chicanne G, Xuereb JM, Marcellin M, Burlet-Schiltz O, Sansonetti PJ, Payrastre B, Tronchère H, TOM1 is a PI5P effector involved in the regulation of endosomal maturation. J Cell Sci 128, 815–827 (2015). [PubMed: 25588840]
7. Viaud J, Lagarrigue F, Ramel D, Allart S, Chicanne G, Ceccato L, Courilleau D, Xuereb JM, Pertz O, Payrastre B, Gaits-Iacovoni F, Phosphatidylinositol 5-phosphate regulates invasion through binding and activation of Tiam1. Nat Commun 5 (2014), doi:10.1038/NCOMMS5080.
8. Hong AW, Meng Z, Plouffe SW, Lin Z, Zhang M, Guan KL, Critical roles of phosphoinositides and NF2 in Hippo pathway regulation. Genes Dev 34, 511–525 (2020). [PubMed: 32115406]
9. Han H, Qi R, Zhou JJ, Ta AP, Yang B, Nakaoka HJ, Seo G, Guan KL, Luo R, Wang W, Regulation of the Hippo pathway by phosphatidic acid-mediated lipid-protein interaction. Mol Cell 72, 328 (2018). [PubMed: 30293781]
10. Lin TY, Ramsamooj S, Perrier T, Liberatore K, Lantier L, Vasan N, Karukurichi K, Hwang SK, Kesicki EA, Kastenhuber ER, Wiederhold T, Yaron TM, Huntsman EM, Zhu M, Ma Y, Paddock MN, Zhang G, Hopkins BD, McGuinness O, Schwartz RE, Ersoy BA, Cantley LC, Johnson JL, Goncalves MD, Epinephrine inhibits PI3Kα via the Hippo kinases. Cell Rep 42 (2023), doi:10.1016/J.CELREP.2023.113535.
11. Poli A, Pennacchio FA, Ghisleni A, di Gennaro M, Lecacheur M, Nastały P, Crestani M, Pramotton FM, Iannelli F, Beznusenko G, Mironov AA, Panzetta V, Fusco S, Sheth B, Poulikakos D, Ferrari A, Gauthier N, Netti PA, Divecha N, Maiuri P, PIP4K2B is mechanoresponsive and controls heterochromatin-driven nuclear softening through UHRF1. Nature Communications 2023 14:1 14, 1–15 (2023).
12. Li FL, Fu V, Liu G, Tang T, Konradi AW, Peng X, Kemper E, Cravatt BF, Franklin JM, Wu Z, Mayfield J, Dixon JE, Gerwick WH, Guan KL, Hippo pathway regulation by phosphatidylinositol transfer protein and phosphoinositides. Nat Chem Biol 18, 1076–1086 (2022). [PubMed: 35788180]
13. Fu M, Hu Y, Lan T, Guan KL, Luo T, Luo M, The Hippo signalling pathway and its implications in human health and diseases. Signal Transduction and Targeted Therapy 2022 7:1 7, 1–20 (2022).
14. Al-Ramahi I, Giridharan SSP, Chen YC, Patnaik S, Safren N, Hasegawa J, de Haro M, Gee AKW, Titus SA, Jeong H, Clarke J, Krainc D, Zheng W, Irvine RF, Barmada S, Ferrer M, Southall N, Weisman LS, Botas J, Marugan JJ, Inhibition of PIP4Kγ ameliorates the pathological effects of mutant huntingtin protein. Elife 6 (2017), doi:10.7554/ELIFE.29123.
15. Chen S, Tjin CC, Gao X, Xue Y, Jiao H, Zhang R, Wu M, He Z, Ellman J, Ha Y, Pharmacological inhibition of PI5P4Kα/β disrupts cell energy metabolism and selectively kills p53-null tumor cells. Proc Natl Acad Sci U S A 118 (2021), doi:10.1073/PNAS.2002486118.
16. Clarke JH, Irvine RF, Evolutionarily conserved structural changes in phosphatidylinositol 5-phosphate 4-kinase (PI5P4K) isoforms are responsible for differences in enzyme activity and localization. Biochemical Journal 454, 49–57 (2013). [PubMed: 23758345]
17. Davis MI, Sasaki AT, Shen M, Emerling BM, Thorne N, Michael S, Pragani R, Boxer M, Sumita K, Takeuchi K, Auld DS, Li Z, Cantley LC, Simeonov A, A homogeneous, high-throughput assay

for phosphatidylinositol 5-phosphate 4-kinase with a novel, rapid substrate preparation. PLoS One 8 (2013), doi:10.1371/JOURNAL.PONE.0054127.

18. Kitagawa M, Liao PJ, Lee KH, Wong J, Shang SC, Minami N, Sampetrean O, Saya H, Lingyun D, Prabhu N, Diam GK, Sobota R, Larsson A, Nordlund P, McCormick F, Ghosh S, Epstein DM, Dymock BW, Lee SH, Dual blockade of the lipid kinase PIP4Ks and mitotic pathways leads to cancer-selective lethality. Nat Commun 8 (2017), doi:10.1038/S41467-017-02287-5.
19. Manz TD, Sivakumaren SC, Ferguson FM, Zhang T, Yasgar A, Seo HS, Ficarro SB, Card JD, Shim H, Miduturu CV, Simeonov A, Shen M, Marto JA, Dhe-Paganon S, Hall MD, Cantley LC, Gray NS, Discovery and Structure-Activity Relationship Study of (Z)-5-Methylenethiazolidin-4-one Derivatives as Potent and Selective Pan-phosphatidylinositol 5-Phosphate 4-Kinase Inhibitors. J Med Chem 63, 4880–4895 (2020). [PubMed: 32298120]
20. Sivakumaren SC, Shim H, Zhang T, Ferguson FM, Lundquist MR, Browne CM, Seo HS, Paddock MN, Manz TD, Jiang B, Hao MF, Krishnan P, Wang DG, Yang TJ, Kwiatkowski NP, Ficarro SB, Cunningham JM, Marto JA, Dhe-Paganon S, Cantley LC, Gray NS, Targeting the PI5P4K Lipid Kinase Family in Cancer Using Covalent Inhibitors. Cell Chem Biol 27, 525–537.e6 (2020). [PubMed: 32130941]
21. Arora GK, Palamiuc L, Emerling BM, Expanding role of PI5P4Ks in cancer: A promising druggable target. FEBS Lett 596, 3–16 (2022). [PubMed: 34822164]
22. Sivakumaren SC, Shim H, Zhang T, Ferguson FM, Lundquist MR, Browne CM, Seo HS, Paddock MN, Manz TD, Jiang B, Hao MF, Krishnan P, Wang DG, Yang TJ, Kwiatkowski NP, Ficarro SB, Cunningham JM, Marto JA, Dhe-Paganon S, Cantley LC, Gray NS, Targeting the PI5P4K Lipid Kinase Family in Cancer Using Covalent Inhibitors. Cell Chem Biol 27, 525–537.e6 (2020). [PubMed: 32130941]
23. Ma S, Meng Z, Chen R, Guan KL, The hippo pathway: Biology and pathophysiology. Annu Rev Biochem 88, 577–604 (2019). [PubMed: 30566373]
24. Couzens AL, Xiong S, Knight JDR, Mao DY, Guettler S, Picaud S, Kurinov I, Filippakopoulos P, Sicheri F, Gingras AC, MOB1 Mediated Phospho-recognition in the Core Mammalian Hippo Pathway. Molecular & Cellular Proteomics 16, 1098–1110 (2017). [PubMed: 28373298]
25. Ni L, Zheng Y, Hara M, Pan D, Luo X, Structural basis for Mob1-dependent activation of the core Mst-Lats kinase cascade in Hippo signaling. Genes Dev 29, 1416–1431 (2015). [PubMed: 26108669]
26. Chan EHY, Nousiainen M, Chalamalasetty RB, Schäfer A, Nigg EA, Sillje HHW, The Ste20-like kinase Mst2 activates the human large tumor suppressor kinase Lats1. Oncogene 2005 24:12 24, 2076–2086 (2005).
27. Vichalkovski A, Gresko E, Cornils H, Hergovich A, Schmitz D, Hemmings BA, NDR Kinase Is Activated by RASSF1A/MST1 in Response to Fas Receptor Stimulation and Promotes Apoptosis. Current Biology 18, 1889–1895 (2008). [PubMed: 19062280]
28. Yuan Z, Lehtinen MK, Merlo P, Villén J, Gygi S, Bonni A, Regulation of neuronal cell death by MST1-FOXO1 signaling. J Biol Chem 284, 11285–11292 (2009). [PubMed: 19221179]
29. Lehtinen MK, Yuan Z, Boag PR, Yang Y, Villén J, Becker EBE, DiBacco S, de la Iglesia N, Gygi S, Blackwell TK, Bonni A, A Conserved MST-FOXO Signaling Pathway Mediates Oxidative-Stress Responses and Extends Life Span. Cell 125, 987–1001 (2006). [PubMed: 16751106]
30. Creasy CL, Ambrose DM, Chernoff J, The Ste20-like protein kinase, Mst1, dimerizes and contains an inhibitory domain. J Biol Chem 271, 21049–21053 (1996). [PubMed: 8702870]
31. Song H, Mak KK, Topol L, Yun K, Hu J, Garrett L, Chen Y, Park O, Chang J, Simpson RM, Wang CY, Gao B, Jiang J, Yang Y, Mammalian Mst1 and Mst2 kinases play essential roles in organ size control and tumor suppression. Proc Natl Acad Sci U S A 107, 1431–1436 (2010). [PubMed: 20080598]
32. Turk BE, Hutti JE, Cantley LC, Determining protein kinase substrate specificity by parallel solution-phase assay of large numbers of peptide substrates. Nat Protoc 1, 375–379 (2006). [PubMed: 17406259]
33. Won DH, Inoue T, Wei SP, Man LK, Byung OP, Wandless TJ, Meyer T, PI(3,4,5)P3 and PI(4,5)P2 lipids target proteins with polybasic clusters to the plasma membrane. Science (1979) 314, 1458–1461 (2006).

34. Hao Y, Chun A, Cheung K, Rashidi B, Yang X, Tumor Suppressor LATS1 Is a Negative Regulator of Oncogene YAP*. Journal of Biological Chemistry 283, 5496–5509 (2008). [PubMed: 18158288]

35. Liu CY, Zha ZY, Zhou X, Zhang H, Huang W, Zhao D, Li T, Chan SW, Lim CJ, Hong W, Zhao S, Xiong Y, Lei QY, Guan KL, The hippo tumor pathway promotes TAZ degradation by phosphorylating a phosphodegron and recruiting the SCF{beta}-TrCP E3 ligase. J Biol Chem 285, 37159–37169 (2010). [PubMed: 20858893]

36. Lei Q-Y, Zhang H, Zhao B, Zha Z-Y, Bai F, Pei X-H, Zhao S, Xiong Y, Guan K-L, TAZ promotes cell proliferation and epithelial-mesenchymal transition and is inhibited by the hippo pathway. Mol Cell Biol 28, 2426–2436 (2008). [PubMed: 18227151]

37. Dong J, Feldmann G, Huang J, Wu S, Zhang N, Comerford SA, Gayyed MFF, Anders RA, Maitra A, Pan D, Elucidation of a universal size-control mechanism in Drosophila and mammals. Cell 130, 1120–1133 (2007). [PubMed: 17889654]

38. Zhao B, Ye X, Yu J, Li L, Li W, Li S, Yu J, Lin JD, Wang CY, Chinnaiyan AM, Lai ZC, Guan KL, TEAD mediates YAP-dependent gene induction and growth control. Genes Dev 22, 1962–1971 (2008). [PubMed: 18579750]

39. Tian W, Yu J, Tomchick DR, Pan D, Luo X, Structural and functional analysis of the YAP-binding domain of human TEAD2. Proc Natl Acad Sci U S A 107, 7293–7298 (2010). [PubMed: 20368466]

40. Dupont S, Morsut L, Aragona M, Enzo E, Giulitti S, Cordenonsi M, Zanconato F, Le Digabel J, Forcato M, Bicciato S, Elvassore N, Piccolo S, Role of YAP/TAZ in mechanotransduction. Nature 474, 179–184 (2011). [PubMed: 21654799]

41. Cordenonsi M, Zanconato F, Azzolin L, Forcato M, Rosato A, Frasson C, Inui M, Montagner M, Parenti AR, Poletti A, Daidone MG, Dupont S, Basso G, Bicciato S, Piccolo S, The Hippo transducer TAZ confers cancer stem cell-related traits on breast cancer cells. Cell 147, 759–772 (2011). [PubMed: 22078877]

42. Li Y, Ye X, Tan C, Hongo JA, Zha J, Liu J, Kallop D, Ludlam MJC, Pei L, Axl as a potential therapeutic target in cancer: role of Axl in tumor growth, metastasis and angiogenesis. Oncogene 2009 28:39 28, 3442–3455 (2009).

43. Goyette MA, Duhamel S, Aubert L, Pelletier A, Savage P, Thibault MP, Johnson RM, Carmeliet P, Basik M, Gaboury L, Muller WJ, Park M, Roux PP, Gratton JP, Côté JF, The Receptor Tyrosine Kinase AXL Is Required at Multiple Steps of the Metastatic Cascade during HER2-Positive Breast Cancer Progression. Cell Rep 23, 1476–1490 (2018). [PubMed: 29719259]

44. Lu G, Du R, Dong J, Sun Y, Zhou F, Feng F, Feng B, Han Y, Shang Y, Cancer associated fibroblast derived SLIT2 drives gastric cancer cell metastasis by activating NEK9. Cell Death & Disease 2023 14:7 14, 1–13 (2023).

45. Lin CJ, Huang WR, Wu CZ, Tseng RC, Changes in SLIT2 expression are associated with the migration of human ovarian clear cell carcinoma cells. Oncol Lett 22 (2021), doi:10.3892/OL.2021.12812.

46. Wang Y, Xu X, Maglic D, Dill MT, Mojumdar K, Ng PKS, Jeong KJ, Tsang YH, Moreno D, Bhavana VH, Peng X, Ge Z, Chen H, Li J, Chen Z, Zhang H, Han L, Du D, Creighton CJ, Mills GB, Caesar-Johnson SJ, Demchok JA, Felau I, Kasapi M, Ferguson ML, Hutter CM, Sofia HJ, Tarnuzzer R, Wang Z, Yang L, Zenklusen JC, Zhang J. (Julia), Chudamani S, Liu J, Lolla L, Naresh R, Pihl T, Sun Q, Wan Y, Wu Y, Cho J, DeFreitas T, Frazer S, Gehlenborg N, Getz G, Heiman DI, Kim J, Lawrence MS, Lin P, Meier S, Noble MS, Saksena G, Voet D, Zhang H, Bernard B, Chambwe N, Dhankani V, Knijnenburg T, Kramer R, Leinonen K, Liu Y, Miller M, Reynolds S, Shmulevich I, Thorsson V, Zhang W, Akbani R, Broom BM, Hegde AM, Ju Z, Kanchi RS, Korkut A, Li J, Liang H, Ling S, Liu W, Lu Y, Ng KS, Rao A, Ryan M, Wang J, Weinstein JN, Zhang J, Abeshouse A, Armenia J, Chakravarty D, Chatila WK, de Bruijn I, Gao J, Gross BE, Heins ZJ, Kundra R, La K, Ladanyi M, Luna A, Nissan MG, Ochoa A, Phillips SM, Reznik E, Sanchez-Vega F, Sander C, Schultz N, Sheridan R, Sumer SO, Sun Y, Taylor BS, Wang J, Zhang H, Anur P, Peto M, Spellman P, Benz C, Stuart JM, Wong CK, Yau C, Hayes DN, Parker JS, Wilkerson MD, Ally A, Balasundaram M, Bowlby R, Brooks D, Carlsen R, Chuah E, Dhalla N, Holt R, Jones SJM, Kasaian K, Lee D, Ma Y, Marra MA, Mayo M, Moore RA, Mungall AJ, Mungall K, Robertson AG, Sadeghi S, Schein JE, Sipahimalani P, Tam A, Thiessen

N, Tse K, Wong T, Berger AC, Beroukhim R, Cherniack AD, Cibulskis C, Gabriel SB, Gao GF, Ha G, Meyerson M, Schumacher SE, Shih J, Kucherlapati MH, Kucherlapati RS, Baylin S, Cope L, Danilova L, Bootwalla MS, Lai PH, Maglinte DT, Van Den Berg DJ, Weisenberger DJ, Auman JT, Balu S, Bodenheimer T, Fan C, Hoadley KA, Hoyle AP, Jefferys SR, Jones CD, Meng S, Mieczkowski PA, Mose LE, Perou AH, Perou CM, Roach J, Shi Y, Simons JV, Skelly T, Soloway MG, Tan D, Veluvolu U, Fan H, Hinoue T, Laird PW, Shen H, Zhou W, Bellair M, Chang K, Covington K, Dinh H, Doddapaneni HV, Donehower LA, Drummond J, Gibbs RA, Glenn R, Hale W, Han Y, Hu J, Korchina V, Lee S, Lewis L, Li W, Liu X, Morgan M, Morton D, Muzny D, Santibanez J, Sheth M, Shinbrot E, Wang L, Wang M, Wheeler DA, Xi L, Zhao F, Hess J, Appelbaum EL, Bailey M, Cordes MG, Ding L, Fronick CC, Fulton LA, Fulton RS, Kandoth C, Mardis ER, McLellan MD, Miller CA, Schmidt HK, Wilson RK, Crain D, Curley E, Gardner J, Lau K, Mallery D, Morris S, Paulauskis J, Penny R, Shelton C, Shelton T, Sherman M, Thompson E, Yena P, Bowen J, Gastier-Foster JM, Gerken M, Leraas KM, Lichtenberg TM, Ramirez NC, Wise L, Zmuda E, Corcoran N, Costello T, Hovens C, Carvalho AL, de Carvalho AC, Fregnani JH, Longatto-Filho A, Reis RM, Scapulatempo-Neto C, Silveira HCS, Vidal DO, Burnette A, Eschbacher J, Hermes B, Noss A, Singh R, Anderson ML, Castro PD, Ittmann M, Huntsman D, Kohl B, Le X, Thorp R, Andry C, Duffy ER, Lyadov V, Paklina O, Setdikova G, Shabunin A, Tavobilov M, McPherson C, Warnick R, Berkowitz R, Cramer D, Feltmate C, Horowitz N, Kibel A, Muto M, Raut CP, Malykh A, Barnholtz-Sloan JS, Barrett W, Devine K, Fulop J, Ostrom QT, Shimmel K, Wolinsky Y, Sloan AE, De Rose A, Giuliante F, Goodman M, Karlan BY, Hagedorn CH, Eckman J, Harr J, Myers J, Tucker K, Zach LA, Deyarmin B, Hu H, Kvecher L, Larson C, Mural RJ, Somiari S, Vicha A, Zelinka T, Bennett J, Iacocca M, Rabeno B, Swanson P, Latour M, Lacombe L, Têtu B, Bergeron A, McGraw M, Staugaitis SM, Chabot J, Hibshoosh H, Sepulveda A, Su T, Wang T, Potapova O, Voronina O, Desjardins L, Mariani O, Roman-Roman S, Sastre X, Stern MH, Cheng F, Signoretti S, Berchuck A, Bigner D, Lipp E, Marks J, McCall S, McLendon R, Secord A, Sharp A, Behera M, Brat DJ, Chen A, Delman K, Force S, Khuri F, Magliocca K, Maithel S, Olson JJ, Owonikoko T, Pickens A, Ramalingam S, Shin DM, Sica G, Van Meir EG, Zhang H, Eijckenboom W, Gillis A, Korpershoek E, Looijenga L, Oosterhuis W, Stoop H, van Kessel KE, Zwarthoff EC, Calatozzolo C, Cuppini L, Cuzzubbo S, DiMeco F, Finocchiaro G, Mattei L, Perin A, Pollo B, Chen C, Houck J, Lohavanichbutr P, Hartmann A, Stoehr C, Stoehr R, Taubert H, Wach S, Wullich B, Kycler W, Murawa D, Wiznerowicz M, Chung K, Edenfield WJ, Martin J, Baudin E, Bubley G, Bueno R, De Rienzo A, Richards WG, Kalkanis S, Mikkelsen T, Noushmehr H, Scarpace L, Girard N, Aymerich M, Campo E, Giné E, Guillermo AL, Van Bang N, Hanh PT, Phu BD, Tang Y, Colman H, Evason K, Dottino PR, Martignetti JA, Gabra H, Juhl H, Akeredolu T, Stepa S, Hoon D, Ahn K, Kang KJ, Beuschlein F, Breggia A, Birrer M, Bell D, Borad M, Bryce AH, Castle E, Chandan V, Cheville J, Copland JA, Farnell M, Flotte T, Giama N, Ho T, Kendrick M, Kocher JP, Kopp K, Moser C, Nagorney D, O'Brien D, O'Neill BP, Patel T, Petersen G, Que F, Rivera M, Roberts L, Smallridge R, Smyrk T, Stanton M, Thompson RH, Torbenson M, Yang JD, Zhang L, Brimo F, Ajani JA, Gonzalez AMA, Behrens C, Bondaruk J, Broaddus R, Czerniak B, Esmaeli B, Fujimoto J, Gershenwald J, Guo C, Lazar AJ, Logothetis C, Meric-Bernstam F, Moran C, Ramondetta L, Rice D, Sood A, Tamboli P, Thompson T, Troncoso P, Tsao A, Wistuba I, Carter C, Haydu L, Hersey P, Jakrot V, Kakavand H, Kefford R, Lee K, Long G, Mann G, Quinn M, Saw R, Scolyer R, Shannon K, Spillane A, Stretch J, Synott M, Thompson J, Wilmott J, Al-Ahmadie H, Chan TA, Ghossein R, Gopalan A, Levine DA, Reuter V, Singer S, Singh B, Tien NV, Broudy T, Mirsaidi C, Nair P, Drwiega P, Miller J, Smith J, Zaren H, Park JW, Hung NP, Kebebew E, Linehan WM, Metwalli AR, Pacak K, Pinto PA, Schiffman M, Schmidt LS, Vocke CD, Wentzensen N, Worrell R, Yang H, Moncrieff M, Goparaju C, Melamed J, Pass H, Botnariuc N, Caraman I, Cernat M, Chemencedji I, Clipca A, Doruc S, Gorincioi G, Mura S, Pirtac M, Stancul I, Tcaciuc D, Albert M, Alexopoulou I, Arnaout A, Bartlett J, Engel J, Gilbert S, Parfitt J, Sekhon H, Thomas G, Rassl DM, Rintoul RC, Bifulco C, Tamakawa R, Urba W, Hayward N, Timmers H, Antenucci A, Facciolo F, Grazi G, Marino M, Merola R, de Krijger R, Gimenez-Roqueplo AP, Piché A, Chevalier S, McKercher G, Birsoy K, Barnett G, Brewer C, Farver C, Naska T, Pennell NA, Raymond D, Schilero C, Smolenski K, Williams F, Morrison C, Borgia JA, Liptay MJ, Pool M, Seder CW, Junker K, Omberg L, Dinkin M, Manikhas G, Alvaro D, Bragazzi MC, Cardinale V, Carpino G, Gaudio E, Chesla D, Cottingham S, Dubina M, Moiseenko F, Dhanasekaran R, Becker KF, Janssen KP, Slotta-Huspenina J, Abdel-Rahman MH, Aziz D, Bell S, Cebulla CM, Davis A, Duell R, Elder JB, Hilty J, Kumar B, Lang J, Lehman NL,

Mandt R, Nguyen P, Pilarski R, Rai K, Schoenfield L, Senecal K, Wakely P, Hansen P, Lechan R, Powers J, Tischler A, Grizzle WE, Sexton KC, Kastl A, Henderson J, Porten S, Waldmann J, Fassnacht M, Asa SL, Schadendorf D, Couce M, Graefen M, Huland H, Sauter G, Schlomm T, Simon R, Tennstedt P, Olabode O, Nelson M, Bathe O, Carroll PR, Chan JM, Disaia P, Glenn P, Kelley RK, Landen CN, Phillips J, Prados M, Simko J, Smith-McCune K, VandenBerg S, Roggin K, Fehrenbach A, Kendler A, Sifri S, Steele R, Jimeno A, Carey F, Forgie I, Mannelli M, Carney M, Hernandez B, Campos B, Herold-Mende C, Jungk C, Unterberg A, von Deimling A, Bossler A, Galbraith J, Jacobus L, Knudson M, Knutson T, Ma D, Milhem M, Sigmund R, Godwin AK, Madan R, Rosenthal HG, Adebamowo C, Adebamowo SN, Boussioutas A, Beer D, Giordano T, Mes-Masson AM, Saad F, Bocklage T, Landrum L, Mannel R, Moore K, Moxley K, Postier R, Walker J, Zuna R, Feldman M, Valdivieso F, Dhir R, Luketich J, Pinero EMM, Quintero-Aguilo M, Carlotti CG, Dos Santos JS, Kemp R, Sankarankuty A, Tirapelli D, Catto J, Agnew K, Swisher E, Creaney J, Robinson B, Shelley CS, Godwin EM, Kendall S, Shipman C, Bradford C, Carey T, Haddad A, Moyer J, Peterson L, Prince M, Rozek L, Wolf G, Bowman R, Fong KM, Yang I, Korst R, Rathmell WK, Fantacone-Campbell JL, Hooke JA, Kovatich AJ, Shriver CD, DiPersio J, Drake B, Govindan R, Heath S, Ley T, Van Tine B, Westervelt P, Rubin MA, Il Lee J, Aredes ND, Mariamidze A, Camargo F, Comprehensive Molecular Characterization of the Hippo Signaling Pathway in Cancer. Cell Rep 25, 1304–1317.e5 (2018). [PubMed: 30380420]

47. Zhang H, Von Gise A, Liu Q, Hu T, Tian X, He L, Pu W, Huang X, He L, Cai CL, Camargo FD, Pu WT, Zhou B, Yap1 is required for endothelial to mesenchymal transition of the atrioventricular cushion. J Biol Chem 289, 18681–18692 (2014). [PubMed: 24831012]
48. Zhang L, Yang S, Chen X, Stauffer S, Yu F, Lele SM, Fu K, Datta K, Palermo N, Chen Y, Dong J, The hippo pathway effector YAP regulates motility, invasion, and castration-resistant growth of prostate cancer cells. Mol Cell Biol 35, 1350–1362 (2015). [PubMed: 25645929]
49. Keune W-J, Jones DR, Divecha N, PtdIns5P and Pin1 in oxidative stress signaling. Adv Biol Regul 53, 179–89 (2013). [PubMed: 23602596]
50. Jones DR, Foulger R, Keune WJ, Bultsma Y, Divecha N, PtdIns5P is an oxidative stress-induced second messenger that regulates PKB activation. FASEB J 27, 1644–1656 (2013). [PubMed: 23241309]
51. Meng Z, Moroishi T, Mottier-Pavie V, Plouffe SW, Hansen CG, Hong AW, Park HW, Mo JS, Lu W, Lu S, Flores F, Yu FX, Halder G, Guan KL, MAP4K family kinases act in parallel to MST1/2 to activate LATS1/2 in the Hippo pathway. Nat Commun 6 (2015), doi:10.1038/NCOMMS9357.
52. Ma B, Chen Y, Chen L, Cheng H, Mu C, Li J, Gao R, Zhou C, Cao L, Liu J, Zhu Y, Chen Q, Wu S, Hypoxia regulates Hippo signalling through the SIAH2 ubiquitin E3 ligase. Nat Cell Biol 17, 95–103 (2015). [PubMed: 25438054]
53. Wu H, Wei L, Fan F, Ji S, Zhang S, Geng J, Hong L, Fan X, Chen Q, Tian J, Jiang M, Sun X, Jin C, Yin ZY, Liu Q, Zhang J, Qin F, Lin KH, Yu JS, Deng X, Wang HR, Zhao B, Johnson RL, Chen L, Zhou D, Integration of Hippo signalling and the unfolded protein response to restrain liver overgrowth and tumorigenesis. Nat Commun 6 (2015), doi:10.1038/NCOMMS7239.
54. Mo JS, Meng Z, Kim YC, Park HW, Hansen CG, Kim S, Lim DS, Guan KL, Cellular energy stress induces AMPK-mediated regulation of YAP and the Hippo pathway. Nat Cell Biol 17, 500–510 (2015). [PubMed: 25751140]
55. Ando T, Arang N, Wang Z, Elena Costea D, Feng X, Goto Y, Izumi H, Gilardi M, Ando K, Gutkind JS, EGFR Regulates the Hippo pathway by promoting the tyrosine phosphorylation of MOB1. , doi:10.1038/s42003-021-02744-4.
56. Turunen SP, von Nandelstadh P, Öhman T, Gucciardo E, Seashore-Ludlow B, Martins B, Rantanen V, Li H, Höpfner K, Östling P, Varjosalo M, Lehti K, FGFR4 phosphorylates MST1 to confer breast cancer cells resistance to MST1/2-dependent apoptosis. Cell Death & Differentiation 2019 26:12 26, 2577–2593 (2019).
57. Pan Z, Tian Y, Zhang B, Zhang X, Shi H, Liang Z, Wu P, Li R, You B, Yang L, Mao F, Qian H, Xu W, YAP signaling in gastric cancer-derived mesenchymal stem cells is critical for its promoting role in cancer progression. Int J Oncol 51, 1055–1066 (2017). [PubMed: 28848999]
58. Overholtzer M, Zhang J, Smolen GA, Muir B, Li W, Sgroi DC, Deng CX, Brugge JS, Haber DA, Transforming properties of YAP, a candidate oncogene on the chromosome 11q22 amplicon. Proc Natl Acad Sci U S A 103, 12405–12410 (2006). [PubMed: 16894141]

59. Diamantopoulou Z, White G, Fadlullah MZH, Dreger M, Pickering K, Maltas J, Ashton G, MacLeod R, Baillie GS, Kouskoff V, Lacaud G, Murray GI, Sansom OJ, Hurlstone AFL, Malliri A, TIAM1 Antagonizes TAZ/YAP Both in the Destruction Complex in the Cytoplasm and in the Nucleus to Inhibit Invasion of Intestinal Epithelial Cells. Cancer Cell 31, 621–634.e6 (2017). [PubMed: 28416184]
60. Oppelt A, Haugsten EM, Zech T, Danielsen HE, Sveen A, Lobert VH, Skotheim RI, Wesche J, PIKfyve, MTMR3 and their product PtdIns5P regulate cancer cell migration and invasion through activation of Rac1. Biochem J 461, 383–390 (2014). [PubMed: 24840251]
61. Grabon A, Bankaitis VA, McDermott MI, The interface between phosphatidylinositol transfer protein function and phosphoinositide signaling in higher eukaryotes. J Lipid Res 60, 242–268 (2019). [PubMed: 30504233]
62. Ile KE, Schaaf G, Bankaitis VA, Phosphatidylinositol transfer proteins and cellular nanoreactors for lipid signaling. Nat Chem Biol 2, 576–83 (2006). [PubMed: 17051233]
63. Grabon A, Orłowski A, Tripathi A, Vuorio J, Javanainen M, Róg T, Lönnfors M, McDermott MI, Siebert G, Somerharju P, Vattulainen I, Bankaitis VA, Dynamics and energetics of the mammalian phosphatidylinositol transfer protein phospholipid exchange cycle. J Biol Chem 292, 14438–14455 (2017). [PubMed: 28718450]
64. Schaaf G, Ortlund EA, Tyeryar KR, Mousley CJ, Ile KE, Garrett TA, Ren J, Woolls MJ, Raetz CRH, Redinbo MR, Bankaitis VA, Functional anatomy of phospholipid binding and regulation of phosphoinositide homeostasis by proteins of the sec14 superfamily. Mol Cell 29, 191–206 (2008). [PubMed: 18243114]
65. Chi ES, Stivison EA, Blind RD, SF-1 Induces Nuclear PIP2. Biomolecules 13, 1509 (2023). [PubMed: 37892191]
66. Sablin EP, Blind RD, Krylova IN, Ingraham JG, Cai F, Williams JD, Fletterick RJ, Ingraham HA, Structure of SF-1 bound by different phospholipids: Evidence for regulatory ligands. Molecular Endocrinology 23 (2009), doi:10.1210/me.2007-0508.
67. Blind RD, Sablin EP, Kuchenbecker KM, Chiu H-J, Deacon AM, Das D, Fletterick RJ, Ingraham HA, The signaling phospholipid PIP 3 creates a new interaction surface on the nuclear receptor SF-1. Proceedings of the National Academy of Sciences 111, 15054–15059 (2014).
68. Bryant JM, Blind RD, Signaling through non-membrane nuclear phosphoinositide binding proteins in human health and disease. J Lipid Res 60, 299–311 (2019). [PubMed: 30201631]
69. Lundquist MR, Goncalves MD, Loughran RM, Possik E, Vijayaraghavan T, Yang A, Pauli C, Ravi A, Verma A, Yang Z, Johnson JL, Wong JCY, Ma Y, Hwang KS-K, Weinkove D, Divecha N, Asara JM, Elemento O, Rubin MA, Kimmelman AC, Pause A, Cantley LC, Emerling BM, Phosphatidylinositol-5-Phosphate 4-Kinases Regulate Cellular Lipid Metabolism By Facilitating Autophagy. Mol Cell 70, 531–544.e9 (2018). [PubMed: 29727621]
70. Ravi A, Palamiuc L, Loughran RM, Triscott J, Arora GK, Kumar A, Tieu V, Pauli C, Reist M, Lew RJ, Houlihan SL, Fellmann C, Metallo C, Rubin MA, Emerling BM, PI5P4Ks drive metabolic homeostasis through peroxisome-mitochondria interplay. Dev Cell 56, 1661–1676.e10 (2021). [PubMed: 33984270]
71. Greener JG, Kandathil SM, Jones DT, Deep learning extends de novo protein modelling coverage of genomes using iteratively predicted structural constraints. Nat Commun 10, 3977 (2019). [PubMed: 31484923]
72. Källberg M, Wang H, Wang S, Peng J, Wang Z, Lu H, Xu J, Template-based protein structure modeling using the RaptorX web server. Nat Protoc 7, 1511–1522 (2012). [PubMed: 22814390]
73. Xu J, Distance-based protein folding powered by deep learning. Proc Natl Acad Sci U S A 116, 16856–16865 (2019). [PubMed: 31399549]
74. Schenkelberg CD, Bystroff C, InteractiveROSETTA: a graphical user interface for the PyRosetta protein modeling suite. Bioinformatics 31, 4023–4025 (2015). [PubMed: 26315900]
75. Jumper J, Evans R, Pritzel A, Green T, Figurnov M, Ronneberger O, Tunyasuvunakool K, Bates R, Žídek A, Potapenko A, Bridgland A, Meyer C, Kohl SAA, Ballard AJ, Cowie A, Romera-Paredes B, Nikolov S, Jain R, Adler J, Back T, Petersen S, Reiman D, Clancy E, Zielinski M, Steinegger M, Pacholska M, Berghammer T, Bodenstein S, Silver D, Vinyals O, Senior AW, Kavukcuoglu

K, Kohli P, Hassabis D, Highly accurate protein structure prediction with AlphaFold. Nature 596, 583–589 (2021). [PubMed: 34265844]

76. Dallakyan S, Olson AJ, Small-molecule library screening by docking with PyRx. Methods Mol Biol 1263, 243–250 (2015). [PubMed: 25618350]
77. Jo S, Kim T, Iyer VG, Im W, CHARMM-GUI: a web-based graphical user interface for CHARMM.J Comput Chem 29, 1859–1865 (2008). [PubMed: 18351591]
78. Ryckaert J, Ryckaert J, Ciccotti G, Berendsen HJC, Numerical integration of the Cartesian equations of motion of a system with constraints: molecular dynamics of n-alkanes. J. COMPUT. PHYS, 327–341 (1977).
79. Darden T, York D, Pedersen L, Particle mesh Ewald: An N· log (N) method for Ewald sums in large systems. J Chem Phys 98, 10089–10092 (1993).
80. Essmann U, Perera L, Berkowitz ML, Darden T, Lee H, Pedersen LG, A smooth particle mesh Ewald method. J Chem Phys 103, 8577–8593 (1995).
81. Case DA, Cerutti DS, Cheatham III TE, Darden TA, Duke RE, Giese TJ, Gohlke H, Goetz AW, Greene D, Homeyer N, AMBER17. 2017. San Fr. Univ. Calif (2018).
82. Lee J, Hitzenberger M, Rieger M, Kern NR, Zacharias M, Im W, CHARMM-GUI supports the Amber force fields. J Chem Phys 153, 35103 (2020).
83. Roe DR, Cheatham TE, PTRAJ and CPPTRAJ: Software for Processing and Analysis of Molecular Dynamics Trajectory Data. J Chem Theory Comput 9, 3084–3095 (2013). [PubMed: 26583988]
84. V Hammond GR, Schiavo G, Irvine RF, Immunocytochemical techniques reveal multiple, distinct cellular pools of PtdIns4P and PtdIns(4,5)P(2). Biochem J 422, 23–35 (2009). [PubMed: 19508231]
85. Martin M, Cutadapt removes adapter sequences from high-throughput sequencing reads. EMBnet J 17, 10–12 (2011).
86. Dobin A, Davis CA, Schlesinger F, Drenkow J, Zaleski C, Jha S, Batut P, Chaisson M, Gingeras TR, STAR: ultrafast universal RNA-seq aligner. Bioinformatics 29, 15–21 (2013). [PubMed: 23104886]
87. Love MI, Huber W, Anders S, Moderated estimation of fold change and dispersion for RNA-seq data with DESeq2. Genome Biol 15 (2014), doi:10.1186/S13059-014-0550-8.

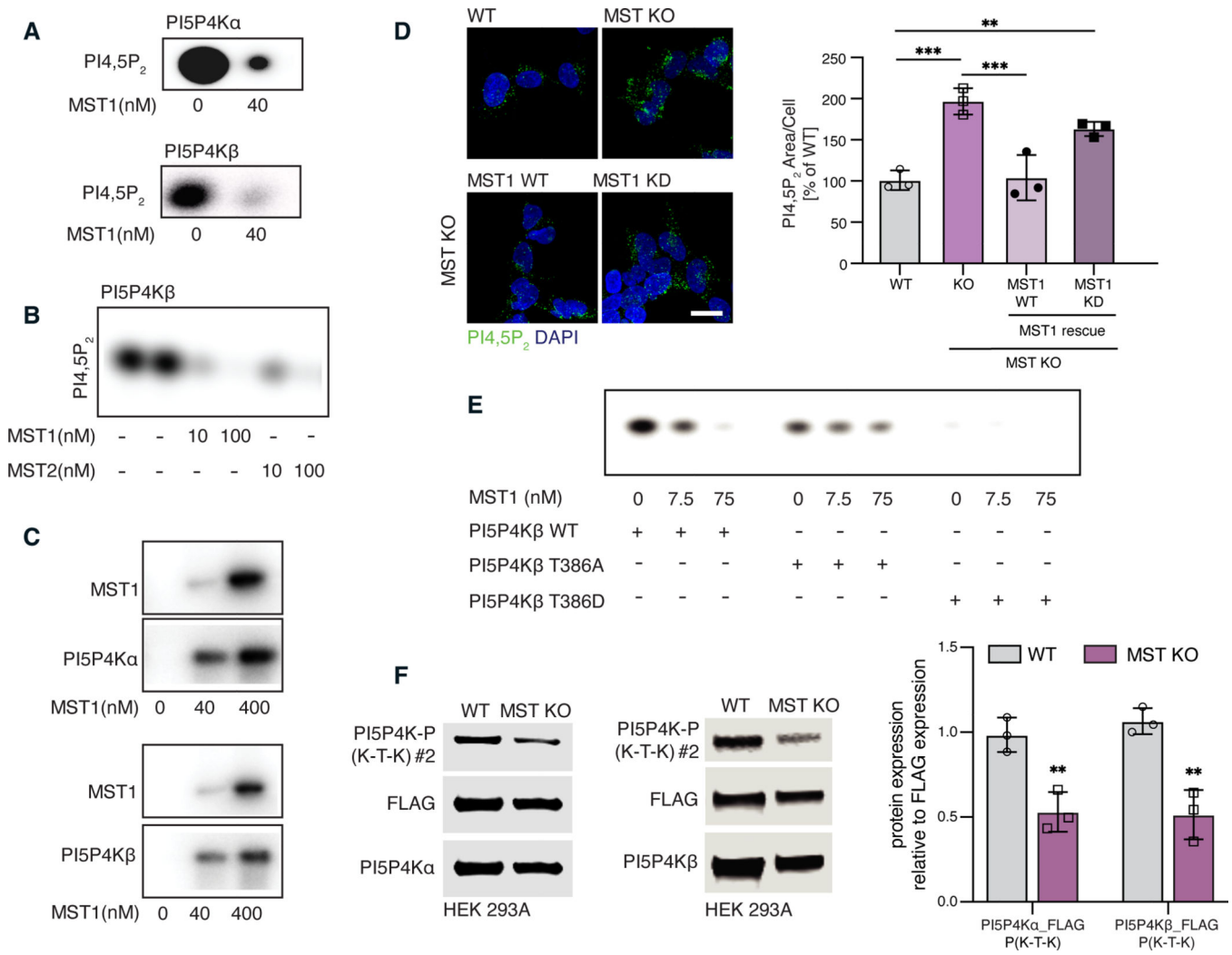

Figure 1. MST and MST2 promote intracellular turnover of PI4,5P_2 by directly phosphorylating PI5P4Ks

(A and B) Thin-layer chromatography (TLC) and autoradiography of in vitro kinase assays in which recombinant PI5P4Kα or PI5P4Kβ was incubated with MST1 (A) and MST2 (B) prior to testing for phosphorylation of PI5P to generate PI4,5P_2 in the presence of radiolabeled ATP. Data are representative of 3 independent experiments. (**C)** SDS-PAGE and autoradiography of in vitro kinase assays in which MST1 was incubated with PI5P4Kα or PI5P4Kβ in the presence of radiolabeled ATP. Data are representative of 3 independent experiments. (**D)** Intracellular pools of PI4,5P_2 assessed by immunofluorescence in WT HEK293A cells, cells with complete CRISPR KO of both MST1 and MST2 (MST KO), and MST KO cells expressing WT MST1 (MST1 WT) or kinase-dead MST1 (MST1 KD). Nuclei are stained with DAPI. Area occupied by PI4,5P_2/cell area was quantified in ImageJ and presented in the adjacent graph as area % of WT. A minimum of 20 cells/experiment/group obtained from n=3 independent experiments were quantified. One-way ANOVA followed by Bonferroni correction, *** p≤ 0.001, ** p≤ 0.01. Scale bar, 50μm. (**E)** TLC and autoradiography of in vitro kinase assays testing for generation of PI4,5P_2 from PI5P by human PI5P4Kβ WT, T386A (phospho-null) and T386D (phospho-mimetic) in the presence

of increasing amounts of MST1. Data are representative of 3 independent experiments. **(F)** Western blotting for FLAG and PI5P4Ks phosphorylated at Thr^{386} (PI5P4Kβ numbering) in WT or MST KO HEK 293A cells expressing FLAG-tagged PI5P4Kα or PI5P4Kβ. Western Blots were quantified from n=3 independent experiments (right, Student's t-test, **p<0.01).

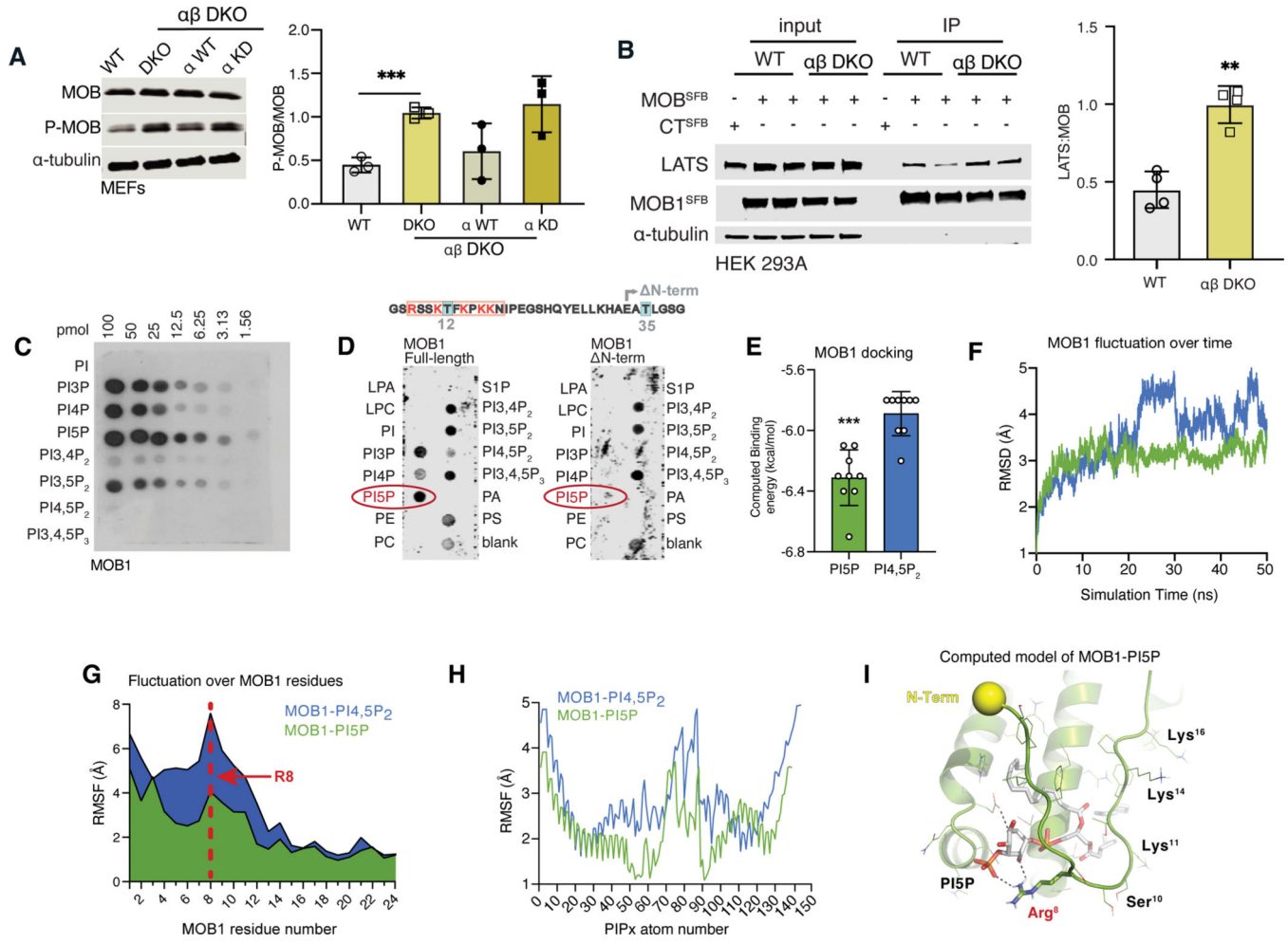

Figure 2. PI5P4K activity inhibits MOB1 phosphorylation and activation of the MOB1-LATS regulatory complex

(A) MOB1 phosphorylation in WT and αβ DKO with or without re-expression of PI5P4Kα (α WT) or kinase-dead PI5P4Kα (α KD) MEFs. Quantified Western blot results are presented as P-MOB1/MOB1 ratio (right), average of 3 independent experiments (one way ANOVA, followed by Welch's correction). **(B)** Co-immunoprecipitation of over-expressed $MOB1^{SFB}$ and endogenous LATS in WT and αβ DKO HEK 293A cells. Quantified Western blot results are represented as LATS1/$MOB1^{SFB}$ ratio averaged over 3 independent experiments (right, Student's t-test, **p<0.01). **(C)** PIP array spotted with eight phosphoinositides at decreasing concentrations and probed with purified human $MOB1^{MYC}$. Representative of 3 independent experiments. **(D)** PIP strip probed with purified human $MOB1^{WT}$ or a truncated ΔN33–216 MOB1 ($MOB1^{\Delta N\text{-term}}$). MOB proteins were immunoblotted with an antibody against His-Tag. Representative of 3 independent experiments. **(E)** Computed binding energies of 9 positions from PyRx blind docking of PI5P and $PI4,5P_2$ (16:0/16:0) to MOB1 (p=0.0001 by unpaired t-test). **(F)** RMSD over 50ns Amber17 MD simulations of MOB1 bound to either PI5P (green) or $PI4,5P_2$ (blue) using the lowest-energy docked structures as the initial state. **(G)** RMSF of the indicated N-terminal MOB1 residues over the entire MD simulation. **(H)** RMSF of the phosphoinositide

atoms over the MD simulation. **(I)** Representative structure from PyRx docking showing interaction of Arg^{8} in MOB1 with the PI5P headgroup. The N-terminus of MOB1 is indicated by a yellow sphere.

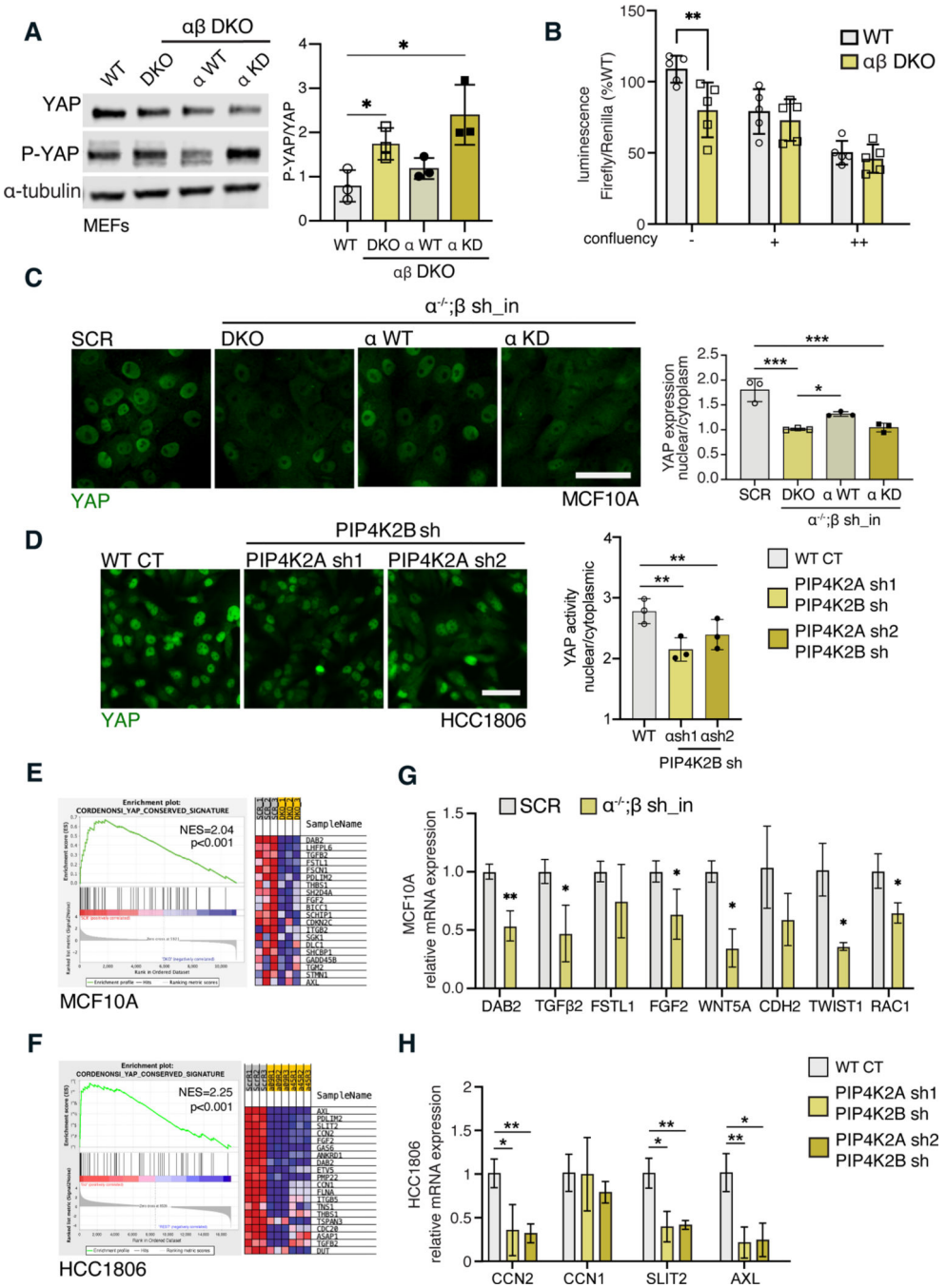

Figure 3. PI5P4K activity is relevant for YAP activation

(A) WT and αβ DKO MEFs reconstituted or not with α WT and α KD were treated with the proteasomal inhibitor MG132 at 5μM or 4 hours and subjected to western blot analysis for phosphorylated YAP. Quantified Western blot results are presented as P-YAP/YAP ratio (right) obtained from 3 independent experiments (Student's t-test, *p≤0.05). **(B)** TEAD luciferase assay performed in WT and αβ DKO HEK 293A cells under increasing confluency conditions. Data represents random luminescence intensities [RLU] obtained from 5 independent experiments (Students t-test, **p≤0.01). **(C)** YAP immunofluorescence

in SCR and DKO MCF10A cells reconstituted with either α WT or α KD MCF10A cells. (scale bar=50μM). Average nuclear: cytoplasmic intensity ratio was quantified from n=3 independent experiments with minimum 20 cells/experiment. Data are presented as a YAP nuclear/YAP cytoplasmic ratio (right). Statistical significance determined by one-way ANOVA followed by Bonferroni, **p≤0.01, *p≤0.05). **(D)** YAP immunofluorescence in α sh_1/β sh, α sh_2/β sh and control (WT CT) HCC1806 breast cancer cells. Average nuclear: cytoplasmic intensity ratio was quantified from 3 independent experiments. Data is represented as a YAP nuclear/YAP cytoplasmic ratio (right). Statistical significance determined by Student's t-test, **p≤0.01, *p≤0.05. **(E)** GSEA RNA-seq analysis for the YAP signature in SCR and DKO MCF10A cells (n=3 biological replicates per group). **(F)** GSEA RNA-seq analysis for the YAP signature in control (WT CT), α sh1/β sh, and α sh2/β sh HCC1806 breast cancer cells (n=3 biological replicates per group). **(G)** qPCR analysis for the relevant top genes and relative values presented in RNA-seq analysis of MCF10A cells (n=3 biological replicates per group). Statistical significance determined by Student T-test, **p≤0.01, *p≤0.05. **(H)** qPCR analysis for the relevant and relative values presented in RNA-seq analysis of HCC1806 cells (n=3 biological replicates per group). Statistical significance determined by Student's t-test, **p≤0.01, *p≤0.05.

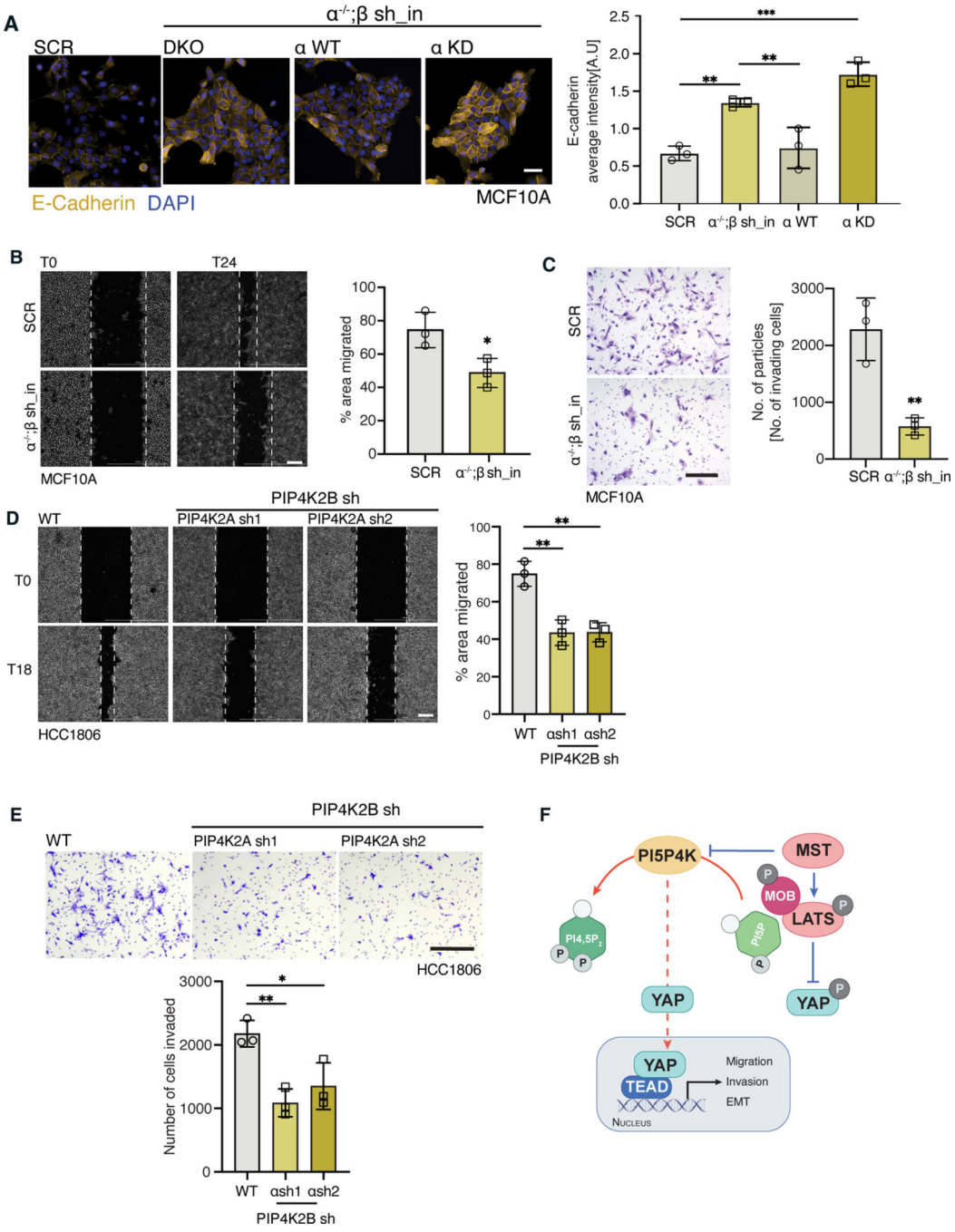

Figure 4. Silencing of PI5P4Ks triggers a decrease in key YAP-related phenotypes

(A) Immunofluorescence of E-cadherin in SCR, DKO, and DKO cells reconstituted with PI5P4Kα (α WT) or kinase dead mutant (α KD) MCF10A cells. Quantification of images are resented as normalized average intensity. E-cadherin in yellow, nuclei (DAPI) in blue. Scale bar=50μm. Statistical significance determined by one-way ANOVA followed by Bonferroni post, ***p≤ 0.0001, **p ≤ 0.001, *p≤0.05. **(B and C)** Wound healing assays performed in a confluent monolayer of SCR and DKO MCF10A epithelial cells (B) and WT CT, α sh1/β sh and α sh2/β sh HCC1806 breast cancer lines (C). Images were taken

every two hours for 24 hours after scratching (T24). Wound areas were quantified from 3 independent experiments with 3–4 technical replicates per experiment and presented as percent area migrated (right). Statistical significance was determined by two-tailed Student's t-test (** $p \leq 0.01$), scale bar=250μm. **(D and E)** SCR and DKO MCF10A cells (D) and WT CT, α sh1/β sh and α sh2/β sh HCC1806 breast cancer cells **(E)** were serum starved overnight and transferred to invasion chambers on top of a matrigel membrane in serum-depleted media. Bottom chamber contained complete media, creating a gradient. 24 hours after transfer, cells were fixed and stained with 0.05% crystal violet. Scale bar=500μm. The total number of cells that migrated over n=3 independent experiments were counted and raw values are presented in the graph. Statistical significance determined by Student's t-test (**$p \leq 0.01$). **(F)** Schematic depicting the interaction between PI5P4Ks and the Hippo pathway. The proposed model shows that through regulation of PI5P pools, the lipid kinase activity of PI5P4Ks modulates the formation of the MOB1-LATS complex, triggering the activation of the downstream target YAP. MST1/2, the protein kinases of the Hippo pathway upstream of LATS1, regulate the activity of PI5P4Ks, thus controlling $PI4,5P_2$/PI5P turnover.